

1   **Iron and Heme Coordinate Erythropoiesis through HRI-Mediated Regulation of**

2   **Protein Translation and Gene Expression**

3   Shuping Zhang<sup>1#</sup>, Alejandra Macias-Garcia<sup>1#</sup>, Jacob C. Ulirsch<sup>2,3,4,5</sup>, Jason Velazquez<sup>1</sup>,

4   Vincent L. Butty<sup>6</sup>, Stuart S. Levine<sup>6</sup>, Vijay G. Sankaran<sup>2,3,4</sup> and Jane-Jane Chen<sup>1\*</sup>

5   <sup>1</sup>Institute for Medical Engineering and Science, Massachusetts Institute of Technology,

6   Cambridge, MA 02139, USA

7   <sup>2</sup> Division of Hematology/Oncology, Boston Children's Hospital, Harvard Medical School,

8   Boston, MA 02115, USA

9   <sup>3</sup>Department of Pediatric Oncology, Dana-Farber Cancer Institute, Harvard Medical

10   School, Boston, MA 02115, USA

11   <sup>4</sup>Broad Institute of Massachusetts Institute of Technology and Harvard, Cambridge, MA

12   02142, USA

13   <sup>5</sup>Program in Biological and Biomedical Sciences, Harvard University, Cambridge, MA

14   02138, USA

15   <sup>6</sup>BioMicro Center, Massachusetts Institute of Technology, Cambridge, MA 02139, USA

16

17   <sup>#</sup> These authors contributed equally to this work

18   \* Corresponding Author: [j-jchen@mit.edu](mailto:j-jchen@mit.edu)

19   **Short Title: Global Heme and HRI-Mediated Translation *in vivo***

20 **Abstract**

21 Iron and heme play central roles in red blood cell production. However, the mechanisms

22 by which iron and heme levels coordinate erythropoiesis remain incompletely understood.

23 HRI is a heme-regulated kinase that controls translation by phosphorylating eIF2 $\alpha$ . Here,

24 we investigate the global impact of iron, heme and HRI on protein translation *in vivo* in

25 murine primary erythroblasts using ribosome profiling. By defining the underlying changes

26 in translation during iron and HRI deficiencies, we validate known regulators of this

27 process, including *Atf4*, and identify novel pathways such as co-regulation of ribosomal

28 protein mRNA translation. Surprisingly, we found that heme and HRI pathways, but not

29 iron-regulated pathways, mediate the major protein translational and transcriptional

30 responses to iron deficiency in erythroblasts *in vivo* and thereby identify previously

31 unappreciated regulators of erythropoiesis. Our genome-wide study uncovers the major

32 impact of the HRI-mediated integrated stress response for the adaptation to iron deficiency

33 anemia.

34

35 **Introduction**

36       Iron deficiency anemia is estimated to affect one-third of the global population (Lopez  
37       et al. 2016). In addition to being key components of hemoglobin, the primary oxygen  
38       transport molecule, cellular iron and heme levels impact globin synthesis and red blood  
39       cell production. Specifically, globin is transcriptionally regulated by BACH1 (BTB Domain  
40       and CNC homolog 1) (Igarashi and Sun 2006) and regulated at the level of protein  
41       translation by HRI (heme-regulated eIF2 $\alpha$  kinase) (Chen 2007), both of which are heme-  
42       sensing proteins.

43       During heme deficiency induced by dietary iron deficiency (ID) in mice, HRI is  
44       activated and phosphorylates the  $\alpha$  subunit of eukaryotic initiation factor eIF2 (eIF2 $\alpha$ ) to  
45       inhibit translation of  $\alpha$ - and  $\beta$ -globin mRNAs, so as to prevent proteotoxicity resulting from  
46       heme-free globin chains (Han et al. 2001). Meanwhile, phosphorylated eIF2 $\alpha$  (eIF2 $\alpha$ P)  
47       selectively enhances the translation of activating transcription factor 4 (*Atf4*) mRNA  
48       (Suragani et al. 2012, Chen 2014). This coordinated translational repression of general  
49       protein synthesis with the specific translational enhancement of *Atf4* mRNA by eIF2 $\alpha$ P is  
50       termed the integrated stress response (ISR) (Harding et al. 2003). ISR is a universal  
51       response to several types of cellular stress (Chen 2014, Pakos-Zebrucka et al. 2016)  
52       initiated by the family of eIF2 $\alpha$  kinase. Besides HRI, mammalian cells have three  
53       additional eIF2 $\alpha$  kinases, which are expressed in distinct tissues to combat specific  
54       physiological stress. PKR responds to viral infection (Kaufman 2000) while GCN2 senses

55 nutrient starvations (Hinnebusch 1996). PERK is activated by endoplasmic reticulum (ER)

56 stress (Ron and Harding 2000). All four eIF2 $\alpha$  kinases respond to oxidative and

57 environmental stresses.

58 In the erythroid lineage, HRI expression increases during differentiation with higher

59 expression in the hemoglobinized erythroblasts (Liu et al. 2008). Starting at the basophilic

60 erythroblast stage, HRI is the predominant eIF2 $\alpha$  kinase, expressed two orders of

61 magnitude higher than the other three eIF2 $\alpha$  kinases (Kingsley et al. 2013), and is

62 responsible for over 90% of eIF2 $\alpha$  phosphorylation (Liu et al. 2008). HRI-ISR signaling is

63 necessary for effective erythropoiesis during ID (Han et al. 2001) and acts by reducing

64 oxidative stress and promoting erythroid differentiation (Suragani et al. 2012, Zhang et al.

65 2018). Furthermore, HRI-ISR represses *in vivo* mTORC1 signaling activated by the

66 elevated erythropoietin (Epo) levels during ID specifically in the erythroid lineage (Zhang

67 et al. 2018). Thus, HRI coordinates two key translation-regulation pathways, eIF2 $\alpha$ P and

68 mTORC1 during ID. However, the exact molecular mechanisms by which iron and heme

69 regulate erythropoiesis are incompletely understood.

70 While transcriptional regulation during erythropoiesis has been studied extensively

71 (Kerenyi and Orkin 2010, An et al. 2014), much less is known about translational control

72 of this process (Mills et al. 2016, Khajuria et al. 2018). Ribosome profiling (Ribo-seq) has

73 emerged as a powerful tool to interrogate translation genome-wide (Ingolia et al. 2009).

74 Here, we performed Ribo-seq and mRNA-seq in primary basophilic erythroblasts to

75 investigate how *in vivo* translation is regulated by iron, heme and HRI in an unbiased  
76 manner to gain a global understanding of the molecular mechanisms governing  
77 erythropoiesis. We hypothesized that by globally surveying the landscape of translational  
78 and concomitant transcriptional changes occurring in the context of HRI deficiency either  
79 in iron replete (+Fe) or deficiency (-Fe) conditions, we could gain important insights into  
80 the mechanisms by which iron and heme can coordinate the process of erythropoiesis.  
81 Our results demonstrate that ISR of HRI-mediated translational regulation and subsequent  
82 ATF4-mediated gene expression is the most highly activated and critical pathway in  
83 developing basophilic erythroblasts during iron-restricted erythropoiesis.

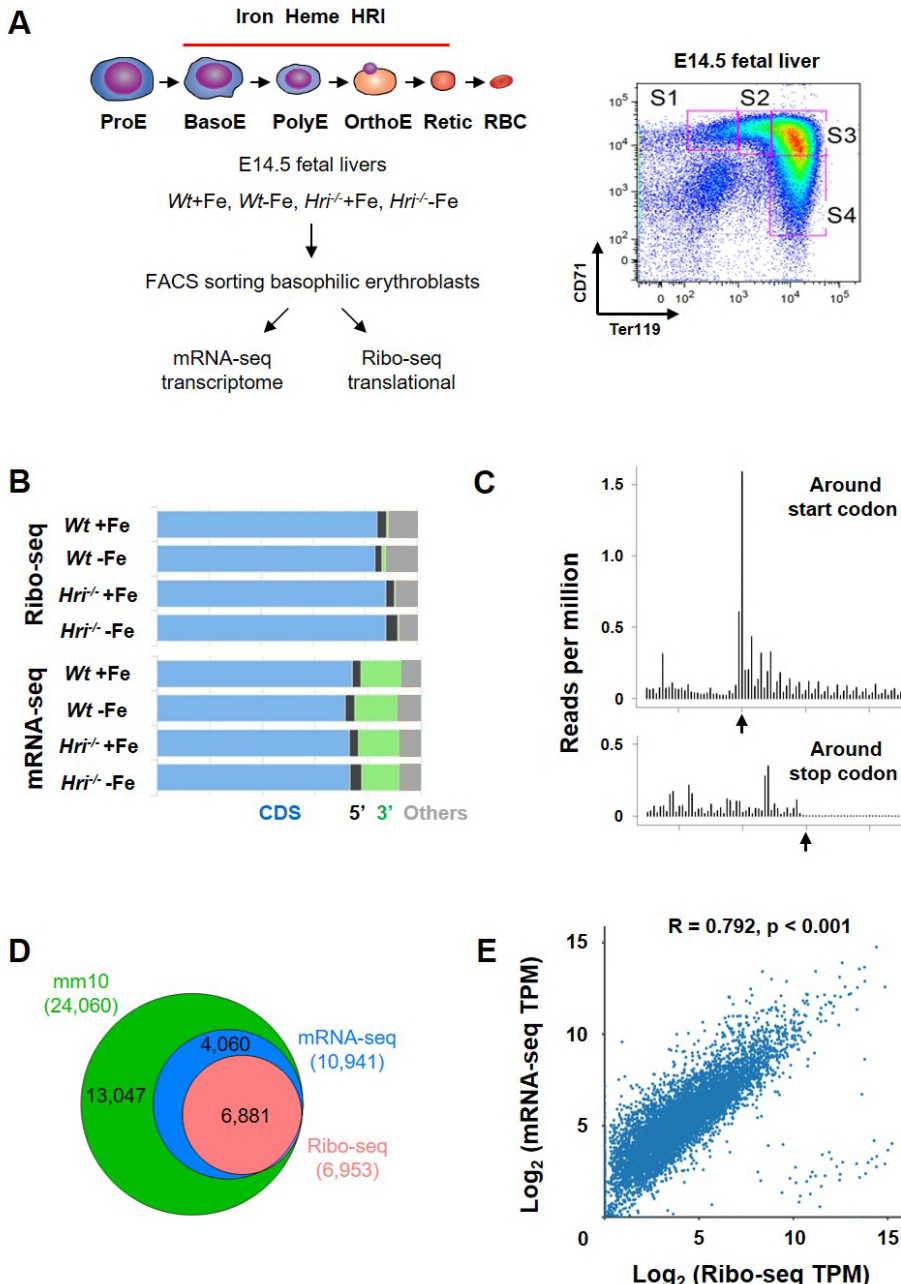
84

## 85 **Results**

86 **Overview of Ribo-seq and mRNA-seq data**

87 Beginning at the basophilic erythroblast stage, erythropoiesis is finely regulated by  
88 iron and heme levels (Chiabrandi, Mercurio, and Tolosano 2014, Muckenthaler et al.  
89 2017). HRI and heme biosynthesis are upregulated, hemoglobin is actively synthesized  
90 (Figure 1A) (Liu et al. 2008, Chen 2014), and the majority of terminal erythroid gene  
91 expression changes have begun (Kerenyi and Orkin 2010, Ulirsch et al. 2014). Thus,  
92 basophilic erythroblasts (thereafter referred as EBs throughout for simplicity) from *Wt*+Fe,  
93 *Wt*-Fe, *Hri*<sup>+/+</sup>-Fe, and *Hri*<sup>-/-</sup>-Fe fetal livers (FLs) were used as sources to generate Ribo-seq  
94 and mRNA-seq libraries for genome-wide analysis of gene expression changes (Figure  
95 1A).

96 **Figure 1. Overview of Ribo-seq and mRNA-seq data**



97

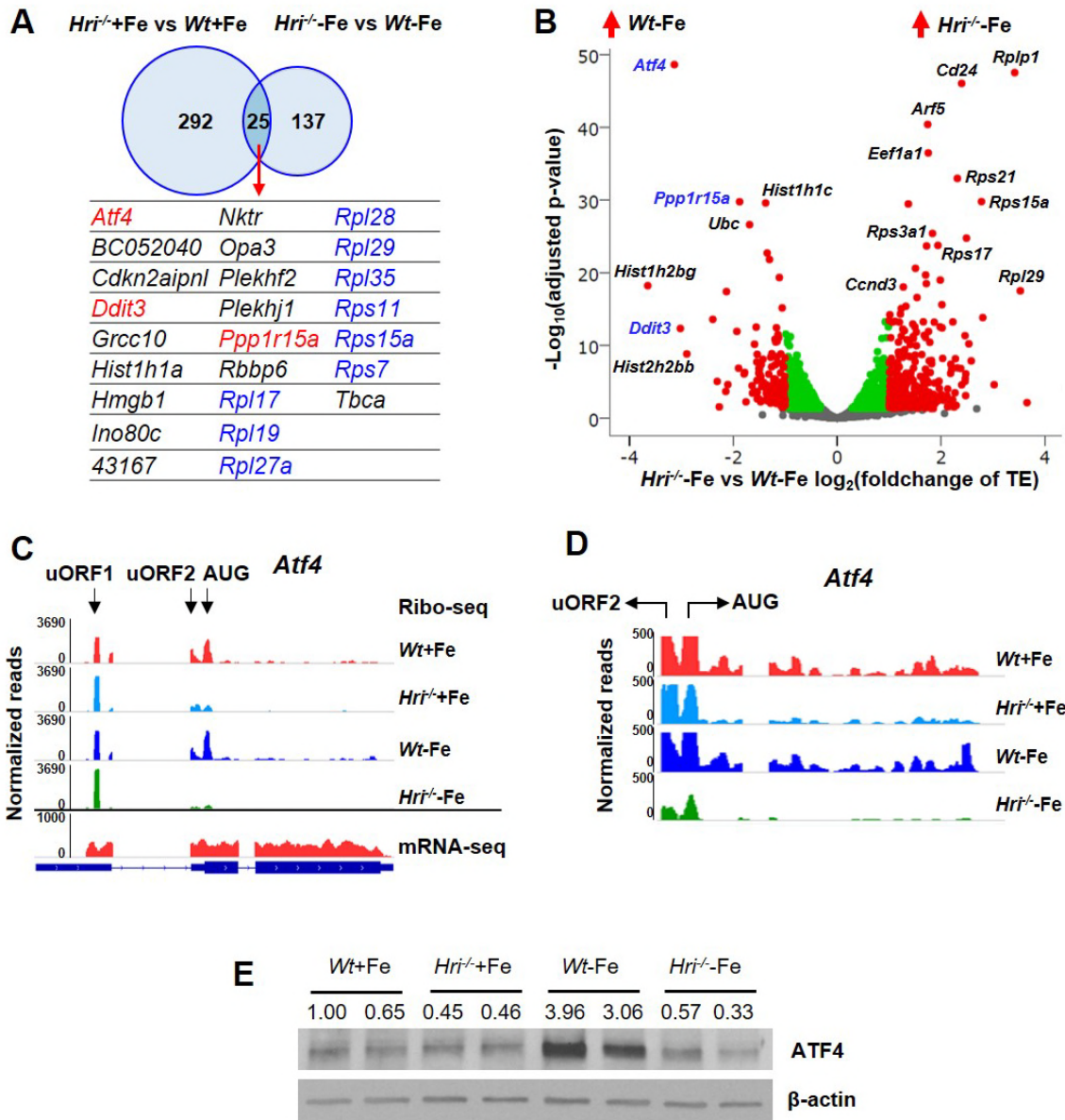
98 **(A)** Illustration of experimental designs. Basophilic erythroblasts (EBs)(S3) from E14.5 FLs of  
99 *Wt*+Fe, *Wt*-Fe, *Hri*<sup>-/-</sup>+Fe and *Hri*<sup>-/-</sup> mice were sorted and subjected to the library preparations of  
100 Ribo-seq and mRNA-seq. **(B)** Distribution of the mapped reads from Ribo-seq and mRNA-seq from  
101 one replica. **(C)** A representative plot of triplet periodicity of Ribo-seq from *Wt*-Fe EBs. Arrow  
102 indicates the start and stop codons. **(D)** Gene coverages of Ribo-seq and mRNA-seq data in the  
103 mouse genome (UCSC, mm10). **(E)** Scatter plot and correlation analysis of log2-transformed TPM  
104 (transcript per million) of Ribo-seq and mRNA-seq data from *Wt*+Fe EBs.  
105 The following table supplement is available for Figure 1: Table supplement 1.

106 After applying standard protocols of quality control and preprocessing to remove  
107 rRNA and tRNA, we obtained 9.7-41.1 (median 26.2) million reads of Ribo-seq and 29.4-  
108 66.6 (median 42.5) million reads of mRNA-seq for subsequent mappings (Table  
109 supplement 1). As expected, most of the reads from both Ribo-seq (84-88%) and mRNA-  
110 seq (72-74%) were mapped to protein coding sequence (CDS) with some of reads  
111 mapped to the 5' and 3' UTR as well as other regions, mostly introns and the regions  
112 around transcription start sites (Figure 1B).

113 Our Ribo-seq data displayed excellent triplet periodicity, CDS enrichment, and limited  
114 3' UTR reads, validating the high quality of ribosome protected fragments (RPFs) that we  
115 obtained (Figure 1B-C). The proportions of reads mapping to 5' UTRs of Ribo-seq data  
116 were similar to those from mRNA-seq (Figure 1B), in agreement with reports of pervasive  
117 translation outside of annotated CDSs (Ingolia et al. 2014). Overall, 62.9% of the  
118 expressed genes in mRNA-seq were detected in Ribo-seq, and therefore appeared to be  
119 actively translated in EBs (Figure 1D). As shown in Figure 1D, 99% of the mRNAs detected  
120 in Ribo-seq data (with reads greater than 25 in at least one of the conditions) were present  
121 in the mRNA-seq data, demonstrating the high quality of our Ribo-seq data and the  
122 correlation of RPFs and mRNAs (Figure 1E).

123 **Upregulation of *in vivo* translation of ISR mRNAs in *Wt* EBs compared to *Hri*<sup>-/-</sup> EBs**  
124 317 mRNAs were significantly differentially translated between *Wt* and *Hri*<sup>-/-</sup> EBs in  
125 +Fe condition (Figure 2A and Table supplement 2), supporting the role of HRI during

126 **Figure 2. Differentially translated mRNAs in HRI and iron deficiencies**



127  
128 **(A)** The significantly differentially translated mRNAs between *Hri<sup>-/-</sup>* and *Wt* EBs in +Fe or -Fe  
129 conditions. **(B)** The volcano plot of differentially translated mRNAs between *Hri<sup>-/-</sup>-Fe* and *Wt-Fe*  
130 EBs. Red dots on the positive end of X-axis indicate significantly differentially translated mRNAs  
131 upregulated in *Hri<sup>-/-</sup>-Fe* EBs while red dots on the negative end of X-axis indicate significantly  
132 differentially translated mRNAs upregulated in *Wt-Fe* EBs. Green and gray dots indicate not  
133 significantly differentially translated mRNAs. TE, translational efficiency. **(C)** Ribosome  
134 occupancies, as visualized using Integrative Genomics Viewer (IGV), of *Atf4* mRNA, with an  
135 enlarged view shown in **(D)**. **(E)** ATF4 protein expression in E14.5 FL cells.  
136 The following supplements are available for Figure 2: Figure supplement 1-2 and Table supplement  
137 2-3.

138 normal fetal erythropoiesis. 25 differentially translated mRNAs were common under both  
139 +Fe and -Fe conditions and included the well-characterized ISR mRNAs, *Atf4*, *Ppp1r15a*,  
140 and *Ddit3* (Figure 2A-B and Figure supplement 1A). *Atf4* mRNA was the most differentially  
141 translated mRNA between *Wt* and *Hri*<sup>-/-</sup> cells during ID (8.8-fold increase in translational  
142 efficiency (TE)), followed by *Ddit3* (8.1-fold) and *Ppp1r15a* (3.7-fold) mRNAs (Figure 2B  
143 and Table supplement 2). Each of these mRNAs contains upstream open reading frames  
144 (uORFs) in their 5' UTR, and the use of which are upregulated by eIF2 $\alpha$ P in cell lines  
145 under endoplasmic reticulum (ER) stress or amino acid starvation (Pavitt and Ron 2012).  
146 We observed HRI-dependent translation regulation of these mRNAs via ribosome  
147 occupancies in uORFs *in vivo* (Figure 2C-D and Figure supplement 1B-C). We also  
148 verified that changes in TE corresponded to change at *Atf4* protein levels in EBs (Figure  
149 2E). In addition, we identified a potential novel candidate mRNA, *Brd2*, which may be

150 regulated by uORFs via HRI-eIF2 $\alpha$ P. TE of *Brd2* mRNA was higher in *Wt*-Fe EBs (2.34-  
151 fold) as compared to *Hri*<sup>-/-</sup>-Fe EBs (Figure supplement 2A). Ribosome occupancies were  
152 observed in putative uORFs at the 5' UTR of *Brd2* mRNA (Figure supplement 2B). We  
153 validated the increased *Brd2* protein expression in *Wt*-Fe EBs compared to *Hri*<sup>-/-</sup>-Fe EBs  
154 (Figure supplement 2C). Depletion of BRD2 expression was shown to inhibit terminal  
155 erythroid differentiation (Stonestrom et al. 2015).

156 Since *Hri* and *Atf4* are among the most highly expressed and efficiently translated  
157 mRNAs in *Wt* EBs (top 3%, Table 1), we investigated whether *Atf4* mRNA was poised for

158 **Table 1** *Hri*, *Ppp1r15a* and *Atf4* mRNAs are highly expressed in basophilic  
159 erythroblasts

Gene Symbol	Rank	mRNA-seq				Ribo-seq			
		Wt+Fe	Hri <sup>-</sup> +Fe	Wt-Fe	Hri <sup>-</sup> -Fe	Wt+Fe	Hri <sup>-</sup> +Fe	Wt-Fe	Hri <sup>-</sup> -Fe
<i>Ftl1</i>	6	10783.2	11396.0	7079.7	8726.3	324.5	416.6	297.1	558.0
<i>Fth1</i>	7	10619.8	10066.0	8485.8	10097.0	2308.3	2866.6	2447.9	4213.9
<i>Alas2</i>	8	9674.5	8269.8	7388.2	9954.1	5545.7	3962.9	4175.6	8487.4
<i>Fech</i>	18	4485.9	3937.3	3358.0	3991.4	1707.6	1647.4	1485.4	2958.5
<i>Tfrc</i>	57	2175.0	2158.2	2436.4	2456.6	1036.8	1436.1	2276.6	2483.1
<i>Klf1</i>	66	1964.8	1848.4	1706.2	1762.1	2687.8	2181.4	2335.0	2010.3
<i>Nfe2</i>	97	1380.9	1159.9	1077.5	1269.8	751.9	724.4	733.4	912.0
<i>Eif2ak1 (Hri)</i>	117	1223.4	1031.2	935.2	1053.3	566.5	461.4	631.6	488.1
<i>Ppp1r15a</i>	120	1222.1	1191.8	997.0	1451.1	751.4	254.8	278.6	158.1
<i>Zfpn1</i>	121	1212.4	1143.1	1045.8	1039.6	89.6	53.3	128.1	100.5
<i>Bcl2l1</i>	156	989.2	745.0	619.7	865.8	225.7	137.1	96.4	130.9
<i>Atf4</i>	202	765.1	717.0	1124.9	729.9	648.2	176.8	466.7	57.7
<i>Gata1</i>	256	618.6	628.7	614.6	600.4	227.7	310.0	335.3	417.7
<i>Foxo3</i>	380	432.9	340.7	274.4	365.9	277.3	195.3	286.4	433.7
<i>Ppp1r15b</i>	908	176.3	184.4	177.9	165.2	15.0	20.7	35.7	23.2
<i>Eif2s1</i>	1345	117.0	132.1	132.2	106.0	52.3	86.5	87.1	80.8
<i>Nfe2l2</i>	1942	75.7	81.4	70.1	76.8	97.0	99.8	109.0	82.7
<i>Ddit3</i>	2016	72.0	65.5	165.0	83.7	112.8	10.3	111.5	13.1
<i>Tfr2</i>	2142	66.6	70.5	73.7	73.0	38.0	25.6	43.8	49.2
<i>Bach1</i>	2478	55.8	52.1	43.3	50.1	15.1	14.3	11.4	9.2
<i>Grb10</i>	3053	41.1	23.3	103.4	23.0	25.3	12.8	75.4	27.1
<i>Ireb2 (Irp2)</i>	3230	37.5	41.2	35.2	38.0	18.1	12.0	27.2	21.2
<i>Atf5</i>	4213	23.2	13.2	316.4	11.5	1.9	0.9	12.9	1.1
<i>Eif2ak2</i>	4520	19.7	20.2	14.3	21.2	16.3	11.7	7.4	13.7
<i>Trib3</i>	5603	10.0	1.7	127.2	4.1	0.5	0.3	20.3	0.8
<i>Eif2ak3</i>	6369	5.0	5.5	6.1	4.9	2.5	2.4	2.0	2.1
<i>Aco1 (Irp1)</i>	6449	4.5	5.6	3.8	5.7	1.3	1.7	3.2	4.7

160 \* mRNAs were ranked by the TPM of each mRNA from mRNA-seq data of Wt+Fe EBs. mRNAs of  
161 interests with respects to erythropoiesis, translation and ISR were compiled to highlight the  
162 abundance of *Hri*, *Ppp1r15a* and *Atf4* mRNAs.

163 Among the four eIF2α kinases, *Hri* (*Eif2ak1*) is most highly expressed in EBs, about 2 orders of the  
164 magnitude of *Pkr* (*Eif2ak2*) and *Perk* (*Eif2ak3*). *Eif2ak4* (*Gcn2*) was expressed at a level lower than  
165 the cut-off.

166 The following table supplement is available for Table 1: Table supplement 4.

167 translational regulation by HRI. *Atf4* mRNA has two well-characterized uORFs in its 5'  
168 UTR, including uORF1 which encodes for 3 amino acids and is translated regardless of  
169 stress and eIF2 $\alpha$ P levels (Pavitt and Ron 2012). We observed that uORF1 had  
170 exceptionally high ribosome occupancy (5.7-fold and 21.3-fold higher than eIF2s1 (eIF2 $\alpha$ )  
171 and *Rps6* initiating AUGs, respectively, Table supplement 3). However, uORF2 and the  
172 canonical ORF of *Atf4* were poorly translated in *Hri*<sup>-/-</sup> compared to *Wt* EBs under both +Fe  
173 and -Fe conditions (Figure 2C-D). Together, these data support the idea that *Atf4* mRNA  
174 is primed for translation by HRI in developing EBs.

175 In contrast, we observed limited changes in the translation of mRNAs containing iron-  
176 responsive elements (IREs) in 5'UTR or at the mRNA levels of TfR1 or DMT1 during ID  
177 or HRI deficiency (Table supplement 4 and Table 1). We found that mRNAs of *Alas2* and  
178 ferritin heavy chain (*Fth1*) were translated in high efficiency in both +Fe and -Fe conditions  
179 (Figure supplement 3 and Table 1). Unexpectedly, our genome-wide study further  
180 demonstrate that *Fth1* mRNA was translated preferentially (7-8 fold) over *Ftl1* mRNA  
181 (Figure supplement 3B and Table 1). Additionally, IRP1 and IRP2 mRNAs were expressed  
182 at low levels and poorly translated in EBs (Table 1).

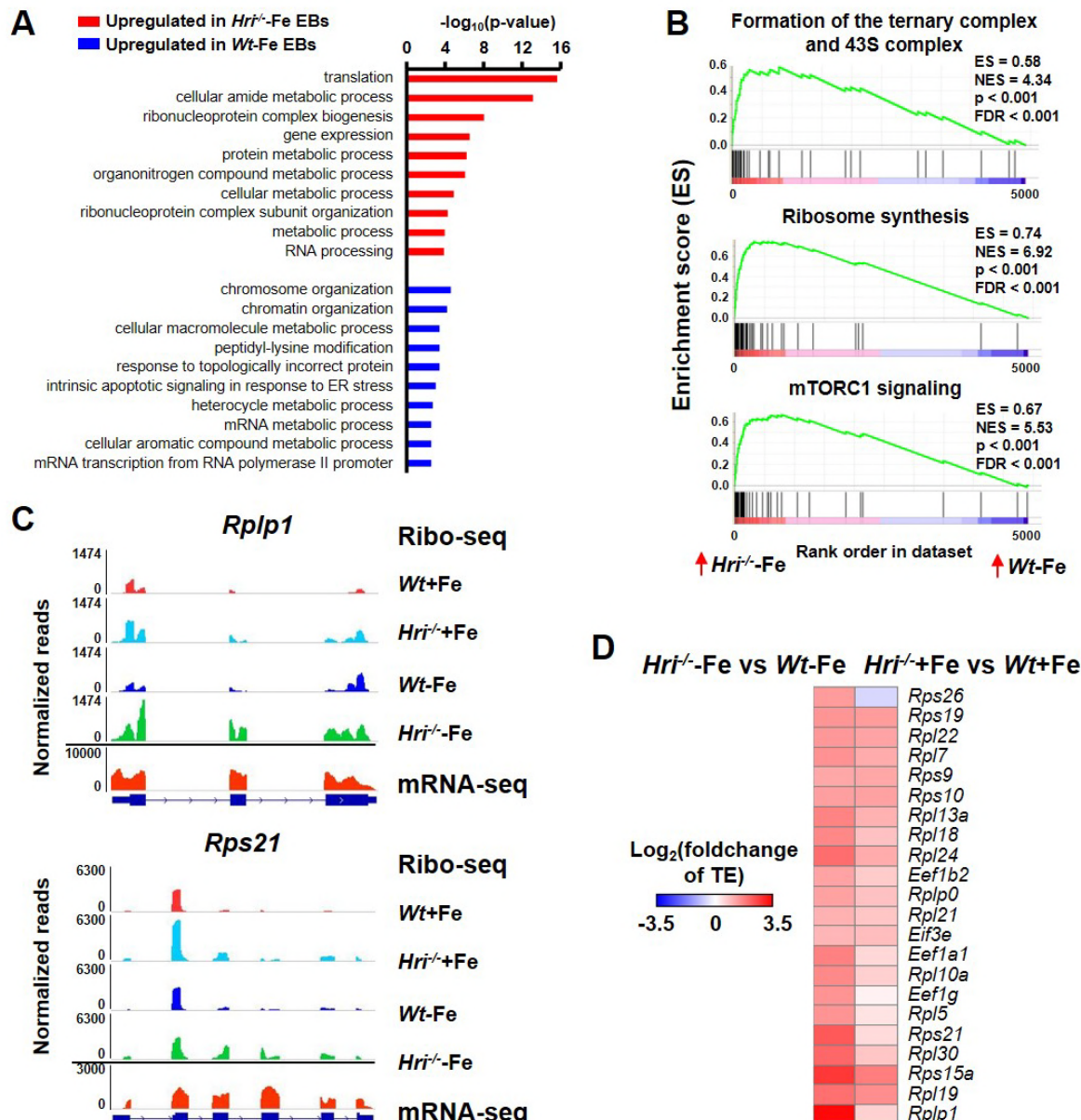
183 These *in vivo* genome-wide results demonstrate that diet-induced ID, sufficient to  
184 induce anemia in mice, does not significantly affect gene expression through IRE/IRPs in  
185 primary developing EBs. Together, our results demonstrate that HRI is a master  
186 translational regulator of key ISR mRNAs *in vivo* in primary EBs especially during ID and

187 suggest that HRI likely regulates the translation of these mRNAs via a uORF-mediated  
188 mechanism.

189 **Upregulation of translation of ribosomal protein mRNAs in *Hri*<sup>-/-</sup>-Fe EBs compared  
190 to *Wt*-Fe EBs**

191 On the other hand, two translational pathways were upregulated in *Hri*<sup>-/-</sup>-Fe EBs as  
192 compared to *Wt*-Fe EBs (Figure 3A-B). First, we found that translation initiation complex  
193 formation was upregulated in *Hri*<sup>-/-</sup>-Fe cells (Figure 3B), consistent with the known function  
194 of HRI-eIF2 $\alpha$ P in ternary and 43S complexes formation (Chen 2007). Second, a number  
195 of ribosomal protein mRNAs and other mTORC1 translational targets were upregulated in  
196 *Hri*<sup>-/-</sup>-Fe EBs compared to *Wt*-Fe EBs (Figure 2A-B and Figure 3B-C). Each of these  
197 ribosomal protein mRNAs have a 5' terminal oligopyrimidine (TOP) motif in their 5' UTR  
198 which permits regulation via mTORC1 signaling (Figure 3D) (Thoreen et al. 2012).  
199 Furthermore, we observed that *Eef1a1* and *Ccnd3*, which have been shown to be  
200 regulated by mTORC1 signaling (Thoreen et al. 2012), were more efficiently translated in  
201 *Hri*<sup>-/-</sup>-Fe cells compared to *Wt*-Fe EBs (Figure 2B). Overall, these genome-wide results  
202 indicate a role of the repressed eIF2 $\alpha$ P and elevated mTORC1 signaling in *Hri*<sup>-/-</sup>-Fe EBs  
203 as compared to *Wt*-Fe EBs.  
204

205 **Figure 3. Analyses of the differentially translated mRNAs between *Wt* and *Hri*<sup>-/-</sup> EBs**



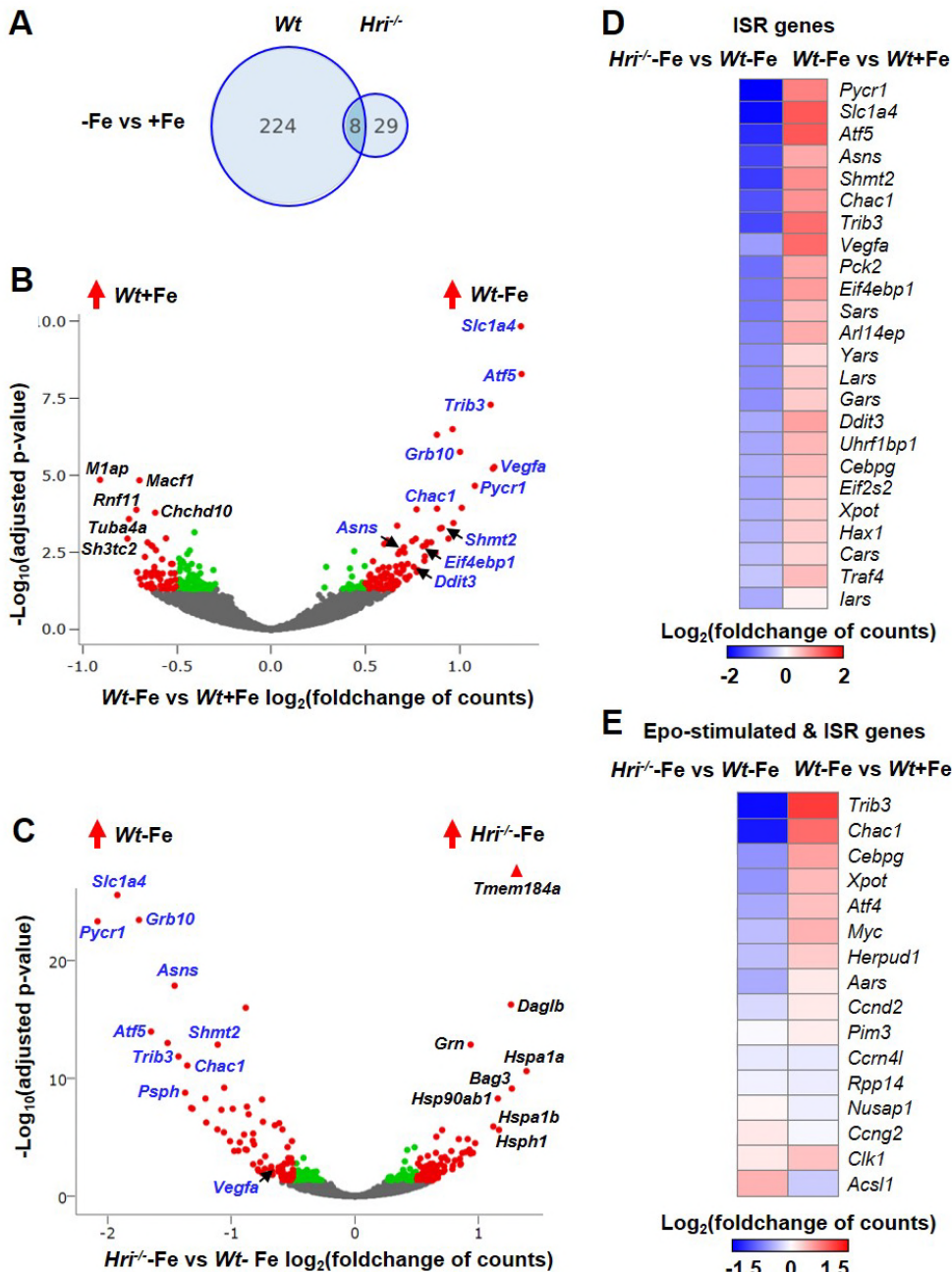
206  
207 **(A)** Gene ontology analysis of the significantly differentially translated mRNAs between *Hri*<sup>-/-</sup>-Fe  
208 and *Wt*-Fe EBs. The top 10 most differentially changed biological processes in *Hri*<sup>-/-</sup>-Fe EBs as  
209 compared to *Wt*-Fe EBs are shown. **(B)** Three upregulated pathways in *Hri*<sup>-/-</sup>-Fe EBs as compared  
210 to *Wt*-Fe EBs revealed by Gene Set Enrichment Analysis. **(C)** IGV-illustration of ribosome  
211 occupancies of two representative ribosome mRNAs, *Rplp1* and *Rps21*. **(D)** The heatmaps of  
212 significantly differentially translated 5'TOP/TOP-like mRNAs, the mTORC1 translational targets.  
213 Positive values of Log<sub>2</sub>(foldchange of TE) indicate upregulated translation in *Hri*<sup>-/-</sup>-Fe EBs as  
214 compared to *Wt*-Fe EBs or in *Hri*<sup>-/-</sup>+Fe EBs as compared to *Wt*+Fe EBs. TE, translational efficiency.  
215

216 **HRI-ATF4 mediated mRNA expression are most highly upregulated in ID**

217 We next investigated the transcriptome impacts of ID and the role of HRI in mediating  
218 the cellular response to this stress. Analysis of mRNA-seq data revealed that there were  
219 substantially more genes that displayed significant differential expression between *Wt*-Fe  
220 and *Wt*+Fe EBs than between *Hri*<sup>+/+</sup>-Fe and *Hri*<sup>-/-</sup>+Fe EBs (232 vs 37, Figure 4A and Table  
221 supplement 5), demonstrating the near-absolute requirement for HRI in regulating the  
222 transcriptional response to ID. The majority of highly induced genes in *Wt*-Fe EBs  
223 compared to *Wt*+Fe EBs were ATF4 target genes, *Slc1a4*, *Atf5*, *Trib3*, *Asns*, *Shmt2*, *Pycr1*  
224 etc (Figure 4B and 4D) (Pakos-Zebrucka et al. 2016). However, these genes were not up  
225 regulated in *Hri*<sup>+/+</sup>-Fe EBs (Figure 4C-D), indicating that HRI is required for activating ISR  
226 in ID (Figure 2). Several of these genes are involved in amino acid metabolism, which is  
227 the top biological process upregulated in *Wt*-Fe EBs compared to *Hri*<sup>+/+</sup>-Fe EBs as shown  
228 by gene ontology analysis (Figure supplement 4A). Furthermore, the expression levels of  
229 these genes were lower in *Hri*<sup>+/+</sup> EBs than *Wt* EBs under +Fe condition (Figure supplement  
230 4B), suggesting that HRI fine-tunes the ISR during iron replete erythropoiesis and thus  
231 has an important role even under normal conditions. Interestingly, some of these ATF4  
232 target genes, most notably *Atf5*, *Trib3* and *Chac1*, are also Epo-stimulated genes (Figure  
233 4E) (Singh et al. 2012), consistent with the interaction of HRI-ISR pathway and Epo  
234 signaling (Zhang et al. 2018).

235

236 **Figure 4. Differentially expressed mRNAs in HRI and iron deficiencies**



237

238 **(A)** Numbers of the significantly differentially expressed mRNAs between -Fe and +Fe conditions  
239 of *Wt* or *Hri*<sup>-/-</sup> EBs. Results were obtained from 3 biological replica. **(B)** Volcano plots of differentially  
240 expressed mRNAs between *Wt*-Fe and *Wt*+Fe or **(C)** between *Hri*<sup>-/-</sup>-Fe and *Wt*-Fe EBs. Red dots  
241 represent the significantly differentially expressed mRNAs. Green and gray dots indicate not  
242 significantly differentially expressed mRNAs. ATF4 target genes are labeled in blue. **(D)** Heatmaps  
243 of significantly differentially expressed ISR-target genes and **(E)** differentially expressed Epo-  
244 stimulated ISR-target genes between *Hri*<sup>-/-</sup>-Fe and *Wt*-Fe EBs or between *Wt*-Fe and *Wt*+Fe EBs.  
245 The following supplements are available for Figure 4: Figure supplement 4, Table supplement 5.

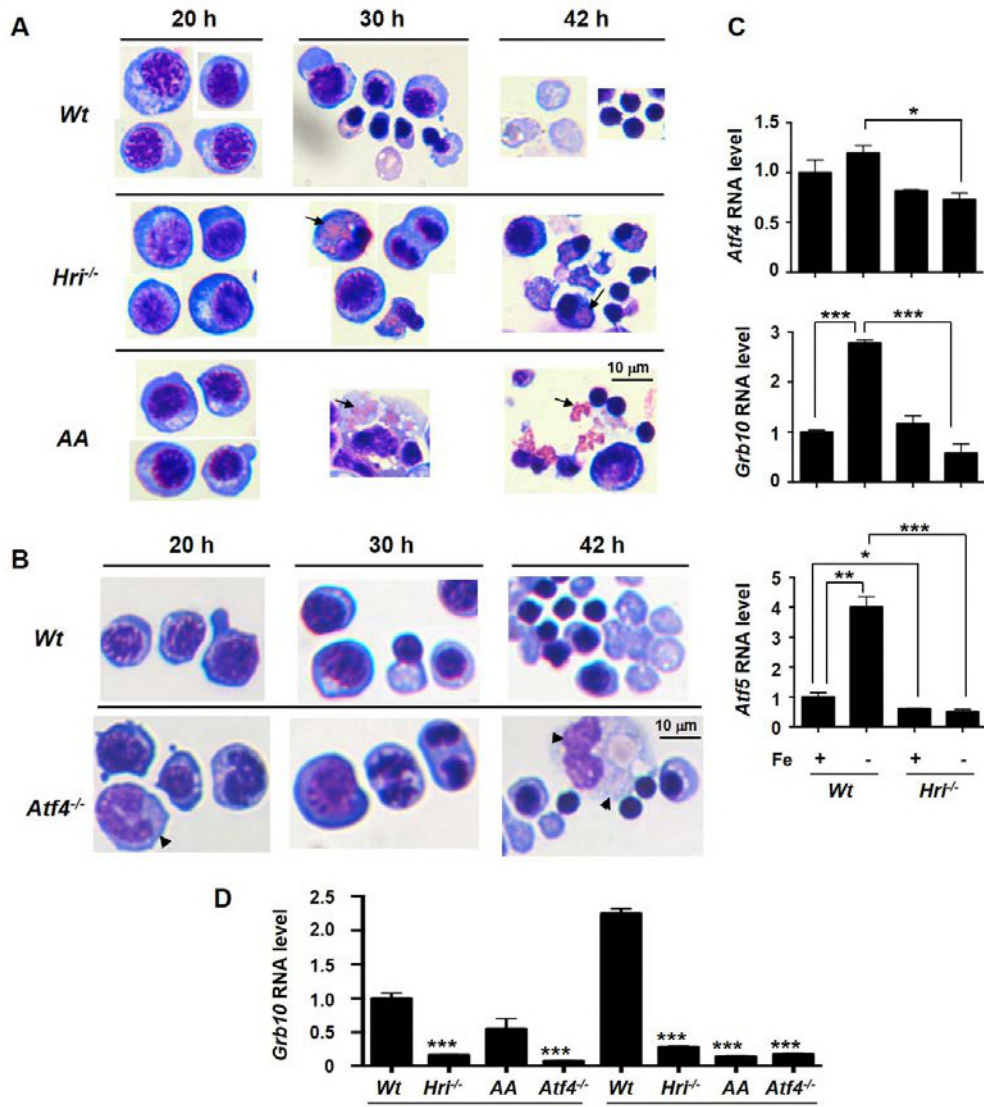
246 **Increased expression of chaperon mRNAs in *Hri*<sup>-/-</sup>-Fe EBs as compared to *Wt*-Fe  
247 EBs**

248 The significantly highly upregulated genes in *Hri*<sup>-/-</sup>-Fe EBs, as compared to *Wt*-Fe EBs,  
249 were predominantly chaperone genes, *Hspa1a*, *Bag3*, *Hsp90ab1*, *Hspa1b* and *Hspf1*  
250 (Figure 4C), supporting the comprehensive upregulation of chaperone expression to  
251 mitigate globin inclusions in *Hri*<sup>-/-</sup>-Fe EBs. GO analysis also showed that processes and  
252 functions related to protein folding were enriched in *Hri*<sup>-/-</sup>-Fe EBs compared to *Wt*-Fe EBs  
253 (Figure supplement 4A). Moreover, *Hri*<sup>-/-</sup>-Fe EBs displayed gene expression  
254 characteristics of G2/M arrest as compared to *Wt*-Fe EBs (Figure supplement 4C),  
255 consistent with the increased cell percentages in G2/M of the cell cycle of splenic *Hri*<sup>-/-</sup>-Fe  
256 erythroid cells (Zhang et al. 2018).

257 **HRI-ISR necessary for fetal liver erythroid differentiation *ex vivo***

258 We have shown previously that HRI-ISR is activated in *ex vivo* FL differentiation  
259 system and that erythroid differentiation of *Hri*<sup>-/-</sup> progenitors is impaired even under +Fe  
260 conditions (Suragani et al. 2012). Here, we show that there was no significant effect of  
261 HRI, eIF2αP, or ATF4 deficiencies on the growth and viability during expansion and up to  
262 20 hours of erythroid differentiation (Figure 5A-B). However, *eIF2α Ala51/Ala51* (AA)  
263 erythroid precursors devoid of eIF2αP accumulated significant amounts of globin  
264 inclusions between 20-30 hours of the differentiation resulting in cell death with fragments  
265 of cell debris (Figure 5A). Similar observation was found in *Hri*<sup>-/-</sup> erythroid precursors

266 **Figure 5. Impaired ex vivo FL differentiation and expression of *Atf4*, *Grb10*, *Atf5*  
267 RNAs in HRI-ISR defective erythroid cells**



268  
269 **(A-B)** Ex vivo erythroid differentiation from HRI, eIF2αP, and ATF4 deficient FL erythroid  
270 progenitors. The representative images of cytopsin slides stained with May-Grunwald/Giemsa  
271 staining. Cells at 20, 30 and 42 hours of erythroid differentiation were shown. AA, universal  
272 eIF2α Ala51/Ala51 knockin resulting in complete ablation of eIF2αP. Arrow indicates globin  
273 inclusions in (A) and arrowhead indicates myeloid cells in (B). Scale bar of 10 μm is indicated.  
274 Numbers of FL differentiation performed, n = 6 for Wt and Hri<sup>-/-</sup>; n = 4 for AA and n = 3 for Atf4<sup>-/-</sup>.  
275 **(C)** Atf4, Grb10 and Atf5 RNA expression in sorted basophilic EBs as illustrate in Figure 1A.  
276 Expression level in Wt+Fe EBs was defined as 1. (n = 3). \*\*\*p < 0.001. **(D)** Grb10 RNA expression  
277 at 20 and 30 hours of ex vivo differentiation of Wt, Hri<sup>-/-</sup>, AA and Atf4 FL erythroid progenitors.  
278 Expression level in Wt EBs at 20 h was defined as 1. For each time point, expression levels in Hri  
279 <sup>-/-</sup>, AA and Atf4 EBs was compared to Wt EBs (n = 3). \*\*\*p < 0.001.

280 (Figure 5A), but less severe since eIF2 $\alpha$ P is completely absence in AA erythroid  
281 precursors while *Hri* $^{-/-}$  cells still have a low level of eIF2 $\alpha$ P. These results underscore the  
282 first and foremost function of HRI-eIF2 $\alpha$ P in inhibiting globin mRNA translation to mitigate  
283 proteotoxicity during FL erythropoiesis (Figure 5A).

284 In contrast, *Atf4* $^{-/-}$  FL erythroid cells did not suffer from proteotoxicity as would be  
285 expected due to the presence of functional HRI-eIF2 $\alpha$ P in inhibiting globin mRNA  
286 translation (Figure 5B). However, differentiation of *Atf4* $^{-/-}$  erythroid precursors at 30 and 42  
287 hours was impaired (Figure 5B). In addition we also observed the presence of myeloid  
288 cells during erythroid differentiation of *Atf4* $^{-/-}$  FL erythroid cells as compared to *Hri* $^{-/-}$  or AA  
289 FL erythroid cells (Figure 5A-B). Together, these results demonstrate that both arms of  
290 ISR, inhibition of globin mRNA translation and enhanced translation of ATF4 mRNA are  
291 required for erythroid differentiation.

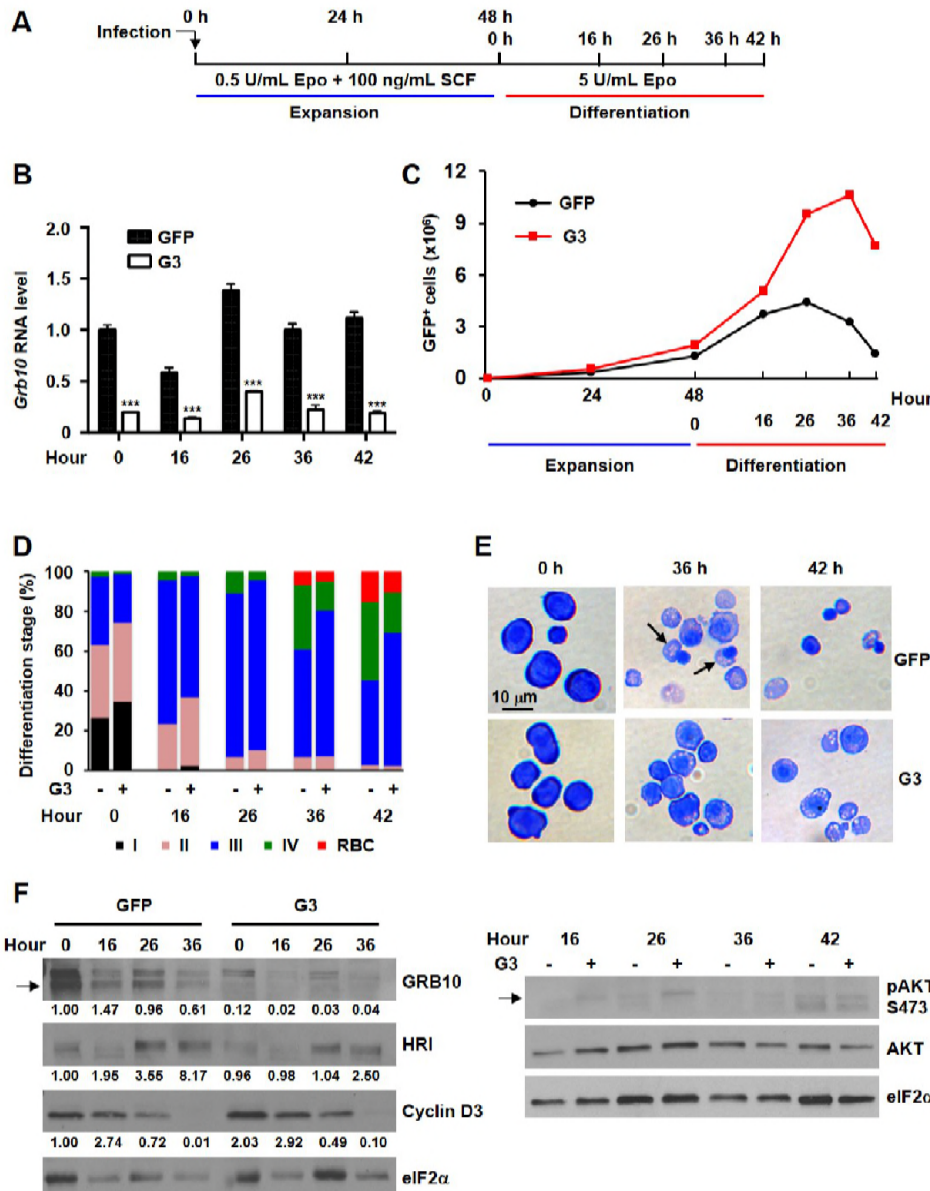
292 ***Grb10* required for late stage erythroid differentiation**

293 Having mapped the genome-wide translational and transcriptional responses to ID,  
294 we set out to characterize the function of one of the top ATF4 target genes, growth factor  
295 receptor-bound protein 10 (*Grb10*) in erythropoiesis. Of all the genes that we identified as  
296 transcriptionally upregulated in *Wt*-Fe, but not *Hri* $^{-/-}$ -Fe EBs, *Grb10* (Figure 4B-C) was  
297 determined to be of particular interest since *Grb10* expression was not increased during  
298 ER stress (Harding et al. 2003), and it is therefore a novel gene that is specifically  
299 regulated by HRI-ISR under systemic ID. Furthermore, *Grb10* has been reported to be

300 part of a feedback mechanism to inhibit growth factor-mediated mTORC1 signaling, such  
301 as insulin (Plasschaert and Bartolomei 2015) and stem cell factor (SCF) (Yan et al. 2016).  
302 We employed *ex vivo* FL differentiation to interrogate the function of *Grb10* in  
303 erythropoiesis.

304 First, we validated that *Grb10* and *Atf5*, but not *Atf4*, RNA expression was increased  
305 in *Wt* EBs, but not *Hri*<sup>-/-</sup> EBs, during ID (Figure 5C). In addition, *Grb10* expression in *Wt*  
306 EBs was increased during *ex vivo* erythroid differentiation from 20 to 30 hours, and was  
307 greatly reduced in *Hri*<sup>-/-</sup>, AA and *Atf4*<sup>-/-</sup> erythroblasts (Figure 5D). We prepared five shRNA  
308 recombinant retroviruses, all of which were able to knockdown *Grb10* RNA expression  
309 greater than 80% during the expansion phase. However, only one, shRNA\_G3, was able  
310 to maintain persistent knockdown of *Grb10* RNA during differentiation (Figure 6A-B, Figure  
311 supplement 5 and Figure supplement 6A). Reduction of *Grb10* expression by shRNA\_G3  
312 both at RNA and protein levels (Figure 6B and 6F) increased cell numbers of differentiating  
313 erythroblasts (Figure 6C and Figure supplement 7A). This increase was first observed  
314 between 16 and 26 hours of differentiation (Figure 6C and Figure supplement 7A), in which  
315 Epo concentration was increased and SCF was withdrawn (Figure 6A). We also observed  
316 increased cyclin D3 expression (Figure 6F), indicating an increase of cells in the S phase  
317 of the cell cycle (Sankaran et al. 2012). Importantly, terminal erythroid differentiation was  
318 inhibited in *Grb10* knockdown cells as indicated by an accumulation of polychromatic  
319 erythroblasts, decrease of orthochromatic erythroblasts, and reduction of enucleation

320 **Figure 6. Grb10 inhibits proliferation and promotes differentiation of erythroblasts**



321

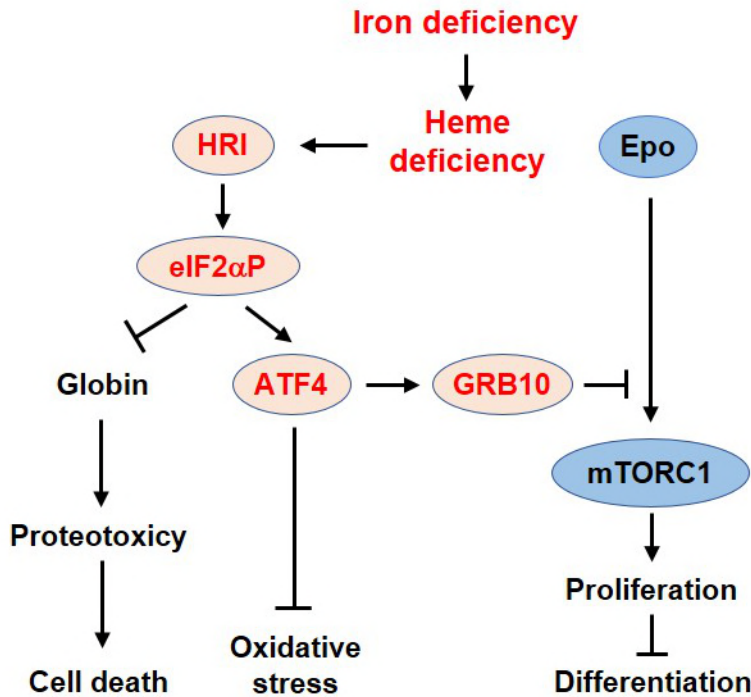
322 **(A)** Designs of shRNA knockdown experiments using Lin-Ter119-CD71<sup>-</sup> FL erythroid progenitors.  
 323 **(B)** Knockdown efficiency of *Grb10* RNA by shRNA\_G3. *Grb10* expression in GFP control at 0 h is  
 324 defined as 1. \*\*\*p < 0.001 (n = 3). **(C)** A representative proliferation of infected GFP<sup>+</sup> cells. **(D)**  
 325 Percentage of GFP<sup>+</sup> cells at different erythroid differentiation stages and **(E)** Cell morphology of  
 326 GFP control and *Grb10* knockdown cells. Scale bar of 10  $\mu$ m is indicated. Arrow indicates  
 327 orthochromatic erythroblast. **(F)** Epo and HRI signaling of GFP control and *Grb10* knockdown cells  
 328 during differentiation. Three *Grb10* knockdown experiments were performed with similar results,  
 329 and the results from a separate experiment are shown in the Figure supplement 7. GFP control,  
 330 infected with retrovirus expressing GFP only; G3, infected with retroviruses expressing shRNA\_G3.  
 331 The following figure supplements are available for Figure 6: Figure supplement 5-7.

332 (Figure 6D-E, Figure supplement 6B-C and Figure supplement 7B-C). Thus, the increased  
333 proliferation but decreased terminal differentiation upon reduction of *Grb10* expression  
334 (Figure 6) recapitulates the hallmarks of ineffective erythropoiesis observed in *Hri*<sup>-/-</sup> mice  
335 in ID (Han et al. 2001, Suragani et al. 2012, Zhang et al. 2018). Mechanistically, we  
336 observed that pAKTS473, a target of Epo signaling, was elevated in *Grb10* knockdown  
337 cells at 16 and 26 hours of differentiation (Figure 6F).

338 These results strengthen our global observation of a potential interaction between  
339 HRI-ISR and the Epo signaling pathway by showing that induction of *Grb10* by HRI-ISR  
340 serves as an important feedback mechanism for Epo signaling, resulting in reduced  
341 proliferation and thus promoting erythroid differentiation during stress erythropoiesis  
342 (Figure 7).

343

344 **Figure 7. Proposed model of the regulation of erythropoiesis by heme and HRI-ISR  
345 pathway during ID**



346  
347 Iron is highly efficiently utilized for heme biosynthesis in developing EBs. There is no apparent IRE-  
348 mediated translational regulation in these cells during ID. Dietary induced systemic ID results in  
349 heme deficiency. HRI is activated in heme deficiency and phosphorylates its substrate eIF2 $\alpha$ . The  
350 first and foremost function of eIF2 $\alpha$ P is to inhibit globin mRNA translation to prevent proteotoxicity  
351 of unfolded heme-free globins. Secondly, eIF2 $\alpha$ P also enhances the translation of *Atf4* mRNA via  
352 regulation by uORFs. *Atf4* mRNA is the most differentially translated mRNA between *Wt* and *Hri*<sup>-/-</sup>  
353 EBs. Increased ATF4 expression then induces gene expression of an array of its target genes,  
354 including *Grb10*. Strikingly, expression of ATF4 target genes is most highly activated in ID and  
355 requires HRI. Thus, global genome-wide gene expression assessment of primary EBs *in vivo*  
356 reveals that HRI-ISR contributes most significantly in adaptation to ID. We have shown previously  
357 that HRI-ISR suppressed the mTORC1 signaling, which is activated by elevated Epo levels in ID  
358 (Zhang et al. 2018). Here, we provide evidence that GRB10 may be one of the molecules in  
359 repressing mTORC1 signaling. GRB10 is necessary to inhibit the proliferation and promote  
360 erythroid differentiation of erythroblasts upon stimulation by Epo.  
361

362     **Discussion**

363         While the specific role of HRI in translational regulation of globin and *Atf4* mRNAs in  
364         erythroid cells has been appreciated, an understanding of the global impact of HRI-  
365         mediated translation on erythropoiesis is lacking. Both iron and heme are necessary for  
366         terminal differentiation and can regulate protein translation, but the effectors that are  
367         critical for mediating responses to variable iron levels have remained undefined. Here, we  
368         report a global, unbiased assessment of iron, heme, and HRI-mediated translational and  
369         transcriptional alterations in primary EBs *in vivo*. Under our diet-induced ID in mice, which  
370         results in iron deficiency anemia, iron *per se* does not affect gene expression in EBs as  
371         translation of IRE-containing mRNAs are not altered during ID. Instead, our study  
372         demonstrates that heme is the major regulator of gene expression, at both the levels of  
373         translation and transcription, during erythropoiesis, as only limited changes of mRNA  
374         expression are observed in *Hri*<sup>-/-</sup> EBs during ID. Thus, heme-regulated translation  
375         mediated by HRI is responsible for tuning gene expression responses to cellular heme  
376         levels during erythropoiesis in ID (Figure 7).

377         Our *in vivo* results in primary EBs are in agreement with the previous report of  
378         Schranzhofer *et al*, demonstrating that *Tfr1* mRNA stability, TfR1 protein expression, and  
379         bindings of IRP1 and IRP2 to IRE are not affected by iron depletion or iron supplement in  
380         differentiating erythroblasts from an immortalized cell line derived from FLs of E12.5 *p53*  
381         <sup>-/-</sup> embryos (Schranzhofer *et al*. 2006). However, inhibition of heme synthesis restores iron-

382 dependent ferritin protein synthesis. Therefore, iron is utilized very efficiently for heme  
383 synthesis such that developing erythroblasts is functionally iron deficient and IRE/IRP is  
384 sensing low iron state. *IRP2*<sup>-/-</sup> mice develop microcytic anemia, demonstrate the essential  
385 role of IRP2 for erythropoiesis (Cooperman et al. 2005, Galy et al. 2005, Ghosh et al.  
386 2008). While the neurodegenerative symptom of *IRP2*<sup>-/-</sup> mice can be restored by IRP1  
387 activation, this is not the case for anemia phenotype. Furthermore, IRP1 activity in  
388 erythroblasts was much lower than that from the brain, and was not activated by treatment  
389 with β-mercaptoethanol (Ghosh et al. 2008). Polycythemia developed in *IRP1*<sup>-/-</sup> mice is not  
390 intrinsic to its deficiency in erythroid lineage but rather is indirectly resulting from the  
391 increased translation of renal HIF2α mRNA, which contains IRE in the 5'UTR, and  
392 subsequent increased Epo production (Ghosh et al. 2013, Anderson et al. 2013, Wilkinson  
393 and Pantopoulos 2013).

394 Recently, it has been shown that ferritin needs to be degraded in order to release its  
395 stored iron (Mancias et al. 2014). Nuclear receptor coactivator 4 (NCOA4) has been  
396 identified as a selective cargo receptor for lysosomal autophagic degradation of ferritin.  
397 Interestingly, NCOA4 binds only to FTH1, but not FTL1 (Mancias et al. 2015). Furthermore,  
398 NCOA4 is essential for erythroid differentiation (Mancias et al. 2015) and *NCOA4*<sup>-/-</sup> mice  
399 developed severe microcytic hypochromic anemia when fed with iron-deficient diet due to  
400 the failure to release iron (Bellelli et al. 2016). This turnover of ferritin protein for the release

401 of iron for heme and hemoglobin synthesis may explain the high rate of *Fth1* mRNA  
402 translation reported here to replenish ferritin protein homeostasis in EBs.

403 Most importantly, both *Hri* and *Atf4* mRNAs were abundantly expressed in EBs at the  
404 level on par with major erythroid transcriptional factors (*Klf1*, *Nfe2* and *Zfpm1*), and highly  
405 occupied by ribosomes, indicating that they are poised to respond to stimuli and stress  
406 during terminal erythroid differentiation. In contrast, *Bach1*, the other erythroid heme-  
407 sensing protein, was expressed at a level about 20-fold lower than *Hri* (Table 1). Our data  
408 further revealed that *Atf4*, the key transcription factor of the ISR pathway, and *Ppp1r15a*  
409 ISR mRNAs, are under exquisite HRI translational control in EBs, likely via mechanisms  
410 involving uORF translation.

411 *Ppp1r15a* gene encodes GADD34, which is a regulatory subunit of PPase1 bringing  
412 eIF2 $\alpha$ P to PPase1 for dephosphorylation in order to reinitiate protein synthesis upon  
413 recovery from stress (Novoa et al. 2001, Kojima et al. 2003, Connor et al. 2001, Brush,  
414 Weiser, and Shenolikar 2003). Homeostasis of eIF2 $\alpha$ P in Ter119 $^+$  erythroid cells is  
415 maintained by HRI and GADD34, both of which are necessary for erythropoiesis. Similar  
416 to *Hri* $^{-/-}$  mice (Han et al. 2001), *Gadd34* $^{-/-}$  mice, develop mild microcytic anemia with slight  
417 splenomegaly under normal conditions (Patterson et al. 2006). In contrast to *Hri* $^{-/-}$  mice  
418 (*Zhang* et al. 2018), *GADD34* $^{-/-}$  mice do not recover completely from iron deficiency  
419 anemia upon iron repletion due to persistent high levels of eIF2 $\alpha$ P and inhibition of globin  
420 protein synthesis (Patterson et al. 2006). It is also noteworthy that *Atf4* $^{-/-}$  mice develop

421 transient anemia during fetal erythropoiesis (Masuoka and Townes 2002) and develop  
422 ineffective erythropoiesis in iron-deficient adult mice (Zhang et al. 2018). These prominent  
423 erythroid phenotypes of *Hri*<sup>-/-</sup>, *Atf4*<sup>-/-</sup> and *Gadd34*<sup>-/-</sup> mice are consistent with the results  
424 reported here on the highest global impact on the gene expression of these two genes by  
425 the activation of HRI-ISR signaling during iron-restricted erythropoiesis. It is to be noted  
426 that a recent study of ribosome profiling study was performed using immortalized FL cell  
427 line upon ER stress and not iron or HRI deficiency (Paolini et al. 2018), in contrast to our  
428 study of primary EBs directly from mice under iron replete and deficient conditions.

429 Our present study identifies several novel regulators of erythropoiesis, providing new  
430 insights into the regulation of stress erythropoiesis. We observed, at a global level,  
431 additional evidence of mTORC1 involvement in translational regulation in the absence of  
432 *Hri*, further supporting the role of HRI-ISR in repressing Epo-mTORC1 signaling to  
433 mitigate ineffective erythropoiesis during ID (Zhang et al. 2018). We provide supporting  
434 evidence that *Grb10* may be one of the ATF4 target genes in inhibiting Epo-mTORC1  
435 signaling in ID. The increased proliferation of differentiating erythroblasts upon knockdown  
436 of *Grb10* reported here is consistent with the growth suppressor function of *Grb10*. *Grb10*,  
437 an imprinted gene, interacts with receptor tyrosine kinases and is a negative regulator of  
438 growth factor signaling (Plasschaert and Bartolomei 2015). Disruption of *Grb10* in mice  
439 results in the overgrowth and enhanced insulin signaling (Charalambous et al. 2003, Smith  
440 et al. 2007, Wang et al. 2007). In hematopoiesis, *Grb10* regulates the self-renewal and

441 regeneration of hematopoietic stem cells (HSCs). *Grb10* deficient HSCs exhibit increased  
442 proliferation that is dependent on SCF-AKT/mTORC1 pathway (Yan et al. 2016),  
443 consistent with our *Grb10* knockdown results.

444 The increased proliferation of differentiating erythroblasts and impairment of terminal  
445 erythroid differentiation upon reduction of *Grb10* expression are the hallmarks of  
446 ineffective erythropoiesis, which characterizes diseases such as thalassemia and the  
447 myelodysplastic syndromes. We have shown earlier that HRI is activated in β-thalassemic  
448 erythroid cells and is necessary to reduce the severity of the disease symptoms in the  
449 mouse model (Han, Fleming, and Chen 2005). Thus, the HRI-ISR-GRB10 pathway may  
450 therefore be exploited for developing novel treatment for these diseases.

451 Induction of fetal hemoglobin (HbF) has been documented to ameliorate the  
452 symptoms of β-thalassemia and sickle cell anemia (Sankaran and Orkin 2013). HRI-ISR  
453 is necessary to reduce the severity of β-thalassemia syndrome in mouse model (Han,  
454 Fleming, and Chen 2005, Suragani et al. 2012). HRI-ISR has been shown to increase  
455 translation of fetal γ-globin mRNA by Hahn and Lowrey in human CD34+ cell culture  
456 through an unknown mechanism (Hahn and Lowrey 2013). Most recently, HRI was  
457 suggested to act as a repressor for HbF production by a domain-focused CRISPRA  
458 genome editing screen (Grevet et al. 2018). HRI depletion diminishes the expression of  
459 BCI11A mRNA, a repressor of γ-globin transcription, although the underlying mechanisms  
460 remain unknown. Interestingly, this HbF repressor action of HRI appears to be unique to

461 human, and not observed in murine erythroid cells (Grevet et al. 2018). HRI deficiency did  
462 not result in significant changes of TE or levels of Bcl11A mRNA in our study report here  
463 (Table supplement 2 and Table supplement 5). The exact role of HRI in HbF production  
464 remains to be clarified.

465 In summary, our genome-wide study reveals the prominent contribution of HRI-ISR  
466 signaling in erythropoiesis and provides molecular insights on HRI-ISR-GRB10 signaling  
467 in the blunted Epo response during ID.

468

469 **Materials and Methods**

470 **Animals and diet-induced iron deficiency**

471 Mice were maintained at the Massachusetts Institute of Technology (MIT) animal  
472 facility, and all experiments were carried out using protocols approved by the Division of  
473 Comparative Medicine, MIT. *Hri*<sup>-/-</sup>, *Atf4*<sup>-/-</sup> and universal *eIF2α Ala51/+* heterozygote  
474 knockin mice were as described previously (Han et al. 2001, Masuoka and Townes 2002,  
475 Scheuner et al. 2001). Diet-induced iron deficiency in mice was as previously described  
476 (Han et al. 2001, Zhang et al. 2018). Mice (8-12 weeks old) were mated for E13.5 or E14.5  
477 fetal livers as sources of erythroid precursors. Under these iron deficient conditions,  
478 embryos were pale and anemic with decreased hematocrits in embryonic blood (Liu et al.  
479 2008).

480 **Isolation of EBs, library preparations, DNA sequencing and genome-wide data  
481 analysis**

482 EBs were sorted using anti-Ter119 and anti-CD71 antibodies by flow cytometry using  
483 FACS Aria (BD Biosciences, San Jose, CA) from E14.5 FLs of *Wt* and *Hri*<sup>-/-</sup> mice  
484 maintained under +Fe or -Fe conditions (Figure 1A). In order to have sufficient EBs for  
485 Ribo-seq library, FLs from embryos of the same mother were pooled then sorted for EBs  
486 as one biological replica. Two (5 million cells each) and three biological replicas (1 million  
487 cells each) of each condition from separate mothers were collected for preparations of  
488 Ribo-seq and mRNA-seq libraries, respectively. The third replica of Ribo-seq using 3

489 million cells was unsuccessful likely due to lower cell numbers. All procedures of labeling  
490 and washing of cells for sorting were carried out at 4°C. Cells were sorted into tubes with  
491 20% fetal bovine serum (FBS, Atlanta Biologicals, Norcross, GA) to help preserving cell  
492 integrity.

493 Ribo-seq libraries were prepared using ARTseq-Ribosome Profiling Kit (Illumina, San  
494 Diego, CA) as previously described (Guo et al. 2010, Ingolia, Lareau, and Weissman 2011)  
495 (see details in Method supplements). Total RNAs were extracted by RNeasy Plus kit  
496 (Qiagen, Germantown, MD) and polyA<sup>+</sup> mRNAs were isolated using an Oligotex mRNA  
497 kit (Qiagen, Germantown, MD). mRNA-seq cDNA libraries were prepared by the MIT  
498 BioMicro Center. cDNA libraries of RPFs and mRNA were sequenced on HiSeq 2000  
499 platform (Illumina, San Diego, CA) at the MIT BioMicro Center. After standard  
500 preprocessing and quality control analysis, reads were mapped to mouse genome mm10  
501 (UCSC) followed by the downstream analyses (see details in Method supplements).

502 All Ribo-seq data and mRNA-seq described in this paper are available at the Gene  
503 Expression Ominibus (<http://www.ncbi.nlm.nih.gov/geo/>) under accession GSE119365.

504 **Enrichment of FL erythroid progenitors for ex vivo culture and differentiation**

505 Erythroid progenitors from E13.5 FLs of *Wt+Fe* embryos were enriched by magnetic  
506 sorting using EasySep Magnet (StemCell Technologies, Vancouver, Canada) as  
507 described (Thom et al. 2014) (see details in Method supplements) and was illustrated in  
508 Figure supplement 5. Purified Lin<sup>-</sup>Ter119<sup>-</sup>CD71<sup>-</sup> erythroid progenitors were cultured in

509 expansion media as described (Thom et al. 2014) for two days at an initial cell density of  
510  $0.5 \times 10^6$  cells per mL. Then, cells were washed and cultured in differentiation media at an  
511 initial cell density of  $1 \times 10^6$  cells per mL. Cells were collected for analysis at different time  
512 points as indicated in the Figure Legends and Figure 6A. Details of expansion media and  
513 differentiation media were described in Method supplements.

514 **Knockdown of *Grb10* expression in FL EBs by retroviral shRNAs**

515 The knockdown of *Grb10* expression was performed by using recombinant  
516 retroviruses containing shRNA-expressing murine stem cell retroviral vector, MSCV-  
517 pgkGFP-U3-U6P-Bbs, a kind gift from the laboratory of Dr. Harvey F. Lodish (MIT). DNA  
518 sequences of five shRNA oligonucleotides (Table supplement 6) targeting different  
519 regions of *Grb10* mRNA were obtained from the Genetic Perturbation Platform of Broad  
520 Institute and synthesized by Integrated DNA Technologies. Preparations of the plasmid  
521 constructs and recombinant retroviruses were performed as described (Hu, Yuan, and  
522 Lodish 2014). Lin<sup>-</sup>Ter119<sup>-</sup>CD71<sup>-</sup> erythroid progenitors enriched from *Wt+Fe* E13.5 FLs  
523 were infected with retroviruses as described (Thom et al. 2014). Cells were expanded for  
524 48 hours after retroviral infections followed by differentiation up to 42 hours as indicated.

525 **Analysis of erythroid differentiation and cell proliferation**

526 Erythroid differentiation was performed by flow cytometry using anti-Ter119 and anti-  
527 CD71 antibodies (BioLegend, San Diego, CA) as described (Zhang et al. 2018) as well as  
528 Draq5 florescent dye (BioLegend, San Diego, CA) for enucleation analysis on FACS LSR

529 II (BD Biosciences, San Jose, CA). 4',6-diamidino-2-phenylindole (DAPI, Roche  
530 Diagnostics, Basel, Switzerland) was used to exclude the dead cells. Data were analyzed  
531 with FlowJo (Tree Star, Ashland, OR). Erythroid differentiation was also analyzed by cell  
532 morphology on cytospin slides stained with May-Grunwald/Giemsa staining (Sigma-  
533 Aldrich, St. Louis, MO). Cell proliferation was determination by counting daily nucleated  
534 cells using crystal violet stain.

535 **RT-qPCR and Western blot analyses**

536 Gene expression was performed by RT-qPCR and Western blot analyses as  
537 previously described (Zhang et al. 2018). Primers were listed in Table supplement 7.  
538 *Gapdh* was used as internal control for RT-qPCR. Antibodies used in Western blot were  
539 described in Table supplement 8.  $\beta$ -actin or eIF2 $\alpha$  was used as a loading control for  
540 western blot.

541 **Statistical Analysis**

542 Independent *t* test (two-tailed) was used to analyze the experimental data. Pearson  
543 correlation analysis was performed to determine the correlation coefficient. Data were  
544 presented in mean  $\pm$  SE. \**p* < 0.05 was considered statistically significant. \*\**p* < 0.01; \*\*\**p*  
545 < 0.001.

546

547 **Acknowledgments**

548 This paper is dedicated to the memory of Irving M. London and his generous and inspiring  
549 mentorship. This work was supported by National Institute of Health Grant RO1 DK087984  
550 (to J-JC), R01 DK103794 and R33 HL120791 (to V.G.S.).

551 **Authorship Contributions**

552 S. Z., A. M-G., J. V. and J-J. C performed experiments. S. Z., J. C. U., V. G. S., V. L. B.  
553 and S. S. L. analyzed sequencing data. S. Z. and J-J. C. wrote the paper. A. M-G., J. C.  
554 U. and V. G. S. edited the paper.

555 **Disclosure of Conflicts of Interest**

556 All authors declare no competing interests.

557

558 **Figure supplements**

- 559 Figure supplement 1. Translational regulation of ISR mRNAs by HRI
- 560 Figure supplement 2. Putative translational regulation of *Brd2* mRNA by HRI in ID
- 561 Figure supplement 3. No significant alteration of translation of ALAS2 and ferritin
- 562 mRNAs in ID
- 563 Figure supplement 4. Analysis of differentially expressed mRNAs
- 564 Figure supplement 5. Enrichment of Lin<sup>-</sup>Ter119<sup>-</sup>CD71<sup>-</sup> erythroid progenitors from *Wt+Fe*
- 565 E13.5 FLs for *ex vivo* experiments
- 566 Figure supplement 6. Effect of knockdown of *Grb10* on FL differentiation *ex vivo*
- 567 Figure supplement 7. Proliferation and differentiation of FL erythroid progenitors upon
- 568 *Grb10* knockdown

569 **Table supplements**

- 570 Table supplement 1. Quality control and mapping of Ribo-seq and mRNA-seq
- 571 Table supplement 2. Complete gene list of differentially translated mRNAs
- 572 Table supplement 3. Higher ribosome occupancy at the AUG of uORF1 in *Atf4* mRNA
- 573 Table supplement 4. No significant changes in TE of iron homeostasis-related genes
- 574 Table supplement 5. Complete gene list of differentially expressed mRNAs
- 575 Table supplement 6. DNA sequences of shRNA oligonucleotides
- 576 Table supplement 7. DNA sequence of qPCR primers
- 577 Table supplement 8. List of antibodies used for Western blot analysis

578 **References**

- 579 An, X., V. P. Schulz, J. Li, K. Wu, J. Liu, F. Xue, J. Hu, N. Mohandas, and P. G. Gallagher.  
580 2014. "Global transcriptome analyses of human and murine terminal erythroid  
581 differentiation." *Blood* 123 (22):3466-77. doi: 10.1182/blood-2014-01-548305.
- 582 Anderson, Sheila A, Christopher P Nizzi, Yuan- I. Chang, Kathryn M Deck, Paul J  
583 Schmidt, Bruno Galy, Alisa Damnernsawad, Aimee T Broman, Christina Kendziora,  
584 Matthias W Hentze, Mark D Fleming, Jing Zhang, and Richard S Eisenstein. 2013. "The  
585 IRP1-HIF-2 $\alpha$  Axis Coordinates Iron and Oxygen Sensing with Erythropoiesis and Iron  
586 Absorption." *Cell Metabolism* 17 (2):282-290. doi:  
587 <https://doi.org/10.1016/j.cmet.2013.01.007>.
- 588 Bellelli, R., G. Federico, A. Matte, D. Colecchia, A. Iolascon, M. Chiariello, M. Santoro,  
589 L. De Franceschi, and F. Carlomagno. 2016. "NCOA4 Deficiency Impairs Systemic Iron  
590 Homeostasis." *Cell Rep* 14 (3):411-421. doi: 10.1016/j.celrep.2015.12.065.
- 591 Brush, M. H., D. C. Weiser, and S. Shenolikar. 2003. "Growth arrest and DNA damage-  
592 inducible protein GADD34 targets protein phosphatase 1 alpha to the endoplasmic  
593 reticulum and promotes dephosphorylation of the alpha subunit of eukaryotic translation  
594 initiation factor 2." *Mol Cell Biol* 23 (4):1292-303.
- 595 Charalambous, Marika, Florentia M. Smith, William R. Bennett, Tracey E. Crew,  
596 Francesca Mackenzie, and Andrew Ward. 2003. "Disruption of the imprinted Grb10  
597 gene leads to disproportionate overgrowth by an Igf2-independent mechanism."  
598 *Proceedings of the National Academy of Sciences* 100 (14):8292.
- 599 Chen, J. J. 2007. "Regulation of protein synthesis by the heme-regulated eIF2alpha kinase:  
600 relevance to anemias." *Blood* 109 (7):2693-9. doi: 10.1182/blood-2006-08-041830.
- 601 Chen, J. J. 2014. "Translational control by heme-regulated eIF2alpha kinase during  
602 erythropoiesis." *Curr Opin Hematol* 21 (3):172-8. doi:  
603 10.1097/MOH.0000000000000030.
- 604 Chiabrandi, D., S. Mercurio, and E. Tolosano. 2014. "Heme and erythropoiesis: more than  
605 a structural role." *Haematologica* 99 (6):973-83. doi: 10.3324/haematol.2013.091991.
- 606 Connor, J. H., D. C. Weiser, S. Li, J. M. Hallenbeck, and S. Shenolikar. 2001. "Growth  
607 arrest and DNA damage-inducible protein GADD34 assembles a novel signaling  
608 complex containing protein phosphatase 1 and inhibitor 1." *Mol Cell Biol* 21  
609 (20):6841-50. doi: 10.1128/mcb.21.20.6841-6850.2001.
- 610 Cooperman, Sharon S., Esther G. Meyron-Holtz, Hayden Olivierre-Wilson, Manik C.  
611 Ghosh, Joseph P. McConnell, and Tracey A. Rouault. 2005. "Microcytic anemia,  
612 erythropoietic protoporphyrina, and neurodegeneration in mice with targeted deletion of  
613 iron-regulatory protein 2." *Blood* 106 (3):1084.
- 614 Galy, Bruno, Dunja Ferring, Belen Minana, Oliver Bell, Heinz G. Janser, Martina  
615 Muckenthaler, Klaus Schümann, and Matthias W. Hentze. 2005. "Altered body iron

- 616 distribution and microcytosis in mice deficient in iron regulatory protein 2 (IRP2)." 617 *Blood* 106 (7):2580.
- 618 Ghosh, Manik C., Wing-Hang Tong, Deliang Zhang, Hayden Ollivierre-Wilson, Anamika 619 Singh, Murali C. Krishna, James B. Mitchell, and Tracey A. Rouault. 2008. "Tempol- 620 mediated activation of latent iron regulatory protein activity prevents symptoms of 621 neurodegenerative disease in IRP2 knockout mice." *Proceedings of the National 622 Academy of Sciences* 105 (33):12028.
- 623 Ghosh, Manik C, De-Liang Zhang, Suh Young Jeong, Gennadiy Kovtunovych, Hayden 624 Ollivierre-Wilson, Audrey Noguchi, Tiffany Tu, Thomas Senecal, Gabrielle Robinson, 625 Daniel R Crooks, Wing-Hang Tong, Kavitha Ramaswamy, Anamika Singh, Brian B 626 Graham, Rubin M Tuder, Zu-Xi Yu, Michael Eckhaus, Jaekwon Lee, Danielle A 627 Springer, and Tracey A Rouault. 2013. "Deletion of Iron Regulatory Protein 1 Causes 628 Polycythemia and Pulmonary Hypertension in Mice through Translational Derepression 629 of HIF2 $\alpha$ ." *Cell Metabolism* 17 (2):271-281. doi: 630 <https://doi.org/10.1016/j.cmet.2012.12.016>.
- 631 Grevet, J. D., X. Lan, N. Hamagami, C. R. Edwards, L. Sankaranarayanan, X. Ji, S. K. 632 Bhardwaj, C. J. Face, D. F. Posocco, O. Abdulmalik, C. A. Keller, B. Giardine, S. Sidoli, 633 B. A. Garcia, S. T. Chou, S. A. Liebhaber, R. C. Hardison, J. Shi, and G. A. Blobel. 634 2018. "Domain-focused CRISPR screen identifies HRI as a fetal hemoglobin regulator 635 in human erythroid cells." *Science* 361 (6399):285-290. doi: 10.1126/science.aao0932.
- 636 Guo, Huili, Nicholas T. Ingolia, Jonathan S. Weissman, and David P. Bartel. 2010. 637 "Mammalian microRNAs predominantly act to decrease target mRNA levels." *Nature* 638 466:835. doi: 10.1038/nature09267  
639 <https://www.nature.com/articles/nature09267#supplementary-information>.
- 640 Hahn, C. K., and C. H. Lowrey. 2013. "Eukaryotic initiation factor 2alpha phosphorylation 641 mediates fetal hemoglobin induction through a post-transcriptional mechanism." *Blood* 642 122 (4):477-85. doi: 10.1182/blood-2013-03-491043.
- 643 Han, A. P., M. D. Fleming, and J. J. Chen. 2005. "Heme-regulated eIF2alpha kinase 644 modifies the phenotypic severity of murine models of erythropoietic protoporphyrina and 645 beta-thalassemia." *J Clin Invest* 115 (6):1562-70. doi: 10.1172/JCI24141.
- 646 Han, A. P., C. Yu, L. Lu, Y. Fujiwara, C. Browne, G. Chin, M. Fleming, P. Leboulch, S. 647 H. Orkin, and J. J. Chen. 2001. "Heme-regulated eIF2alpha kinase (HRI) is required for 648 translational regulation and survival of erythroid precursors in iron deficiency." *Embo j* 20 (23):6909-18. doi: 10.1093/emboj/20.23.6909.
- 649 Harding, H. P., Y. Zhang, H. Zeng, I. Novoa, P. D. Lu, M. Calfon, N. Sadri, C. Yun, B. 650 Popko, R. Paules, D. F. Stojdl, J. C. Bell, T. Hettmann, J. M. Leiden, and D. Ron. 2003. 651 "An integrated stress response regulates amino acid metabolism and resistance to 652 oxidative stress." *Mol Cell* 11 (3):619-33.
- 653

- 654 Hinnebusch, Alan G. 1996. "Translational Control of Gcn4: Gene-Specific Regulation by  
655 Phosphorylation of Eif2." In *Translational Control*, edited by J.W.B. Hershey, M.B.  
656 Mathews and N. Sonenberg, 199-244. Cold Spring Harbor: Cold Spring Harbor  
657 Laboratory Press.
- 658 Hu, W., B. Yuan, and H. F. Lodish. 2014. "Cpeb4-mediated translational regulatory  
659 circuitry controls terminal erythroid differentiation." *Dev Cell* 30 (6):660-72. doi:  
660 10.1016/j.devcel.2014.07.008.
- 661 Igarashi, K., and J. Sun. 2006. "The heme-Bach1 pathway in the regulation of oxidative  
662 stress response and erythroid differentiation." *Antioxid Redox Signal* 8 (1-2):107-18.  
663 doi: 10.1089/ars.2006.8.107.
- 664 Ingolia, N. T., G. A. Brar, N. Stern-Ginossar, M. S. Harris, G. J. Talhouarne, S. E. Jackson,  
665 M. R. Wills, and J. S. Weissman. 2014. "Ribosome profiling reveals pervasive  
666 translation outside of annotated protein-coding genes." *Cell Rep* 8 (5):1365-79. doi:  
667 10.1016/j.celrep.2014.07.045.
- 668 Ingolia, N. T., S. Ghaemmaghami, J. R. Newman, and J. S. Weissman. 2009. "Genome-  
669 wide analysis in vivo of translation with nucleotide resolution using ribosome profiling."  
670 *Science* 324 (5924):218-23. doi: 10.1126/science.1168978.
- 671 Ingolia, N. T., L. F. Lareau, and J. S. Weissman. 2011. "Ribosome profiling of mouse  
672 embryonic stem cells reveals the complexity and dynamics of mammalian proteomes."  
673 *Cell* 147 (4):789-802. doi: 10.1016/j.cell.2011.10.002.
- 674 Ji, Zhe, Ruisheng Song, Aviv Regev, and Kevin Struhl. 2015. "Many lncRNAs, 5'UTRs,  
675 and pseudogenes are translated and some are likely to express functional proteins."  
676 *eLife* 4:e08890. doi: 10.7554/eLife.08890.
- 677 Kaufman, Randal J. 2000. "Double-Stranded RNA-Activated Protein Kinase Pkr." In  
678 *Translational Control of Gene Expression*, edited by J.W.B. Hershey, N. Sonenberg and  
679 M.B. Mathews, 503-28. Cold Spring Harbor: Cold Spring Harbor Laboratory Press.
- 680 Kerenyi, M. A., and S. H. Orkin. 2010. "Networking erythropoiesis." *J Exp Med* 207  
681 (12):2537-41. doi: 10.1084/jem.20102260.
- 682 Khajuria, R. K., M. Munschauer, J. C. Ulirsch, C. Fiorini, L. S. Ludwig, S. K. McFarland,  
683 N. J. Abdulhay, H. Specht, H. Keshishian, D. R. Mani, M. Jovanovic, S. R. Ellis, C. P.  
684 Fulco, J. M. Engreitz, S. Schutz, J. Lian, K. W. Gripp, O. K. Weinberg, G. S. Pinkus, L.  
685 Gehrke, A. Regev, E. S. Lander, H. T. Gazda, W. Y. Lee, V. G. Panse, S. A. Carr, and  
686 V. G. Sankaran. 2018. "Ribosome Levels Selectively Regulate Translation and Lineage  
687 Commitment in Human Hematopoiesis." *Cell*. doi: 10.1016/j.cell.2018.02.036.
- 688 Kingsley, P. D., E. Greenfest-Allen, J. M. Frame, T. P. Bushnell, J. Malik, K. E. McGrath,  
689 C. J. Stoeckert, and J. Palis. 2013. "Ontogeny of erythroid gene expression." *Blood* 121  
690 (6):e5-e13. doi: 10.1182/blood-2012-04-422394.
- 691 Kojima, E., A. Takeuchi, M. Haneda, A. Yagi, T. Hasegawa, K. Yamaki, K. Takeda, S.  
692 Akira, K. Shimokata, and K. Isobe. 2003. "The function of GADD34 is a recovery from

- 693 a shutoff of protein synthesis induced by ER stress: elucidation by GADD34-deficient  
694 mice." *Faseb j* 17 (11):1573-5. doi: 10.1096/fj.02-1184fje.
- 695 Liu, S., S. Bhattacharya, A. Han, R. N. Suragani, W. Zhao, R. C. Fry, and J. J. Chen. 2008.  
696 "Haem-regulated eIF2alpha kinase is necessary for adaptive gene expression in erythroid  
697 precursors under the stress of iron deficiency." *Br J Haematol* 143 (1):129-37. doi:  
698 10.1111/j.1365-2141.2008.07293.x.
- 699 Lopez, Anthony, Patrice Cacoub, Iain C. Macdougall, and Laurent Peyrin-Biroulet. 2016.  
700 "Iron deficiency anaemia." *The Lancet* 387 (10021):907-916. doi: 10.1016/s0140-  
701 6736(15)60865-0.
- 702 Mancias, J. D., L. Pontano Vaites, S. Nissim, D. E. Biancur, A. J. Kim, X. Wang, Y. Liu,  
703 W. Goessling, A. C. Kimmelman, and J. W. Harper. 2015. "Ferritinophagy via NCOA4  
704 is required for erythropoiesis and is regulated by iron dependent HERC2-mediated  
705 proteolysis." *eLife* 4. doi: 10.7554/eLife.10308.
- 706 Mancias, J. D., X. Wang, S. P. Gygi, J. W. Harper, and A. C. Kimmelman. 2014.  
707 "Quantitative proteomics identifies NCOA4 as the cargo receptor mediating  
708 ferritinophagy." *Nature* 509 (7498):105-9. doi: 10.1038/nature13148.
- 709 Masuoka, H. C., and T. M. Townes. 2002. "Targeted disruption of the activating  
710 transcription factor 4 gene results in severe fetal anemia in mice." *Blood* 99 (3):736-45.
- 711 Mills, E. W., J. Wangen, R. Green, and N. T. Ingolia. 2016. "Dynamic Regulation of a  
712 Ribosome Rescue Pathway in Erythroid Cells and Platelets." *Cell Rep* 17 (1):1-10. doi:  
713 10.1016/j.celrep.2016.08.088.
- 714 Muckenthaler, Martina U., Stefano Rivella, Matthias W. Hentze, and Bruno Galy. 2017.  
715 "A Red Carpet for Iron Metabolism." *Cell* 168 (3):344-361. doi:  
716 10.1016/j.cell.2016.12.034.
- 717 Nelson, Jonathan W., Jiri Sklenar, Anthony P. Barnes, and Jessica Minnier. 2017. "The  
718 START App: a web-based RNAseq analysis and visualization resource." *Bioinformatics* 33 (3):447-449. doi: 10.1093/bioinformatics/btw624.
- 720 Novoa, I., H. Zeng, H. P. Harding, and D. Ron. 2001. "Feedback inhibition of the unfolded  
721 protein response by GADD34-mediated dephosphorylation of eIF2alpha." *J Cell Biol*  
722 153 (5):1011-22.
- 723 Pakos-Zebrucka, Karolina, Izabela Koryga, Katarzyna Mnich, Mila Ljubic, Afshin Samali,  
724 and Adrienne M. Gorman. 2016. "The integrated stress response." *EMBO reports* 17  
725 (10):1374-1395. doi: 10.15252/embr.201642195.
- 726 Palam, L. R., J. Gore, K. E. Craven, J. L. Wilson, and M. Korc. 2015. "Integrated stress  
727 response is critical for gemcitabine resistance in pancreatic ductal adenocarcinoma."  
728 *Cell Death & Disease* 6:e1913. doi: 10.1038/cddis.2015.264
- 729 <https://www.nature.com/articles/cddis2015264#supplementary-information>.
- 730 Paolini, Nahuel A., Kat S. Moore, Franca M. di Summa, Ivo F. A. C. Fokkema, Peter A.  
731 C. 't Hoen, and Marieke von Lindern. 2018. "Ribosome profiling uncovers selective

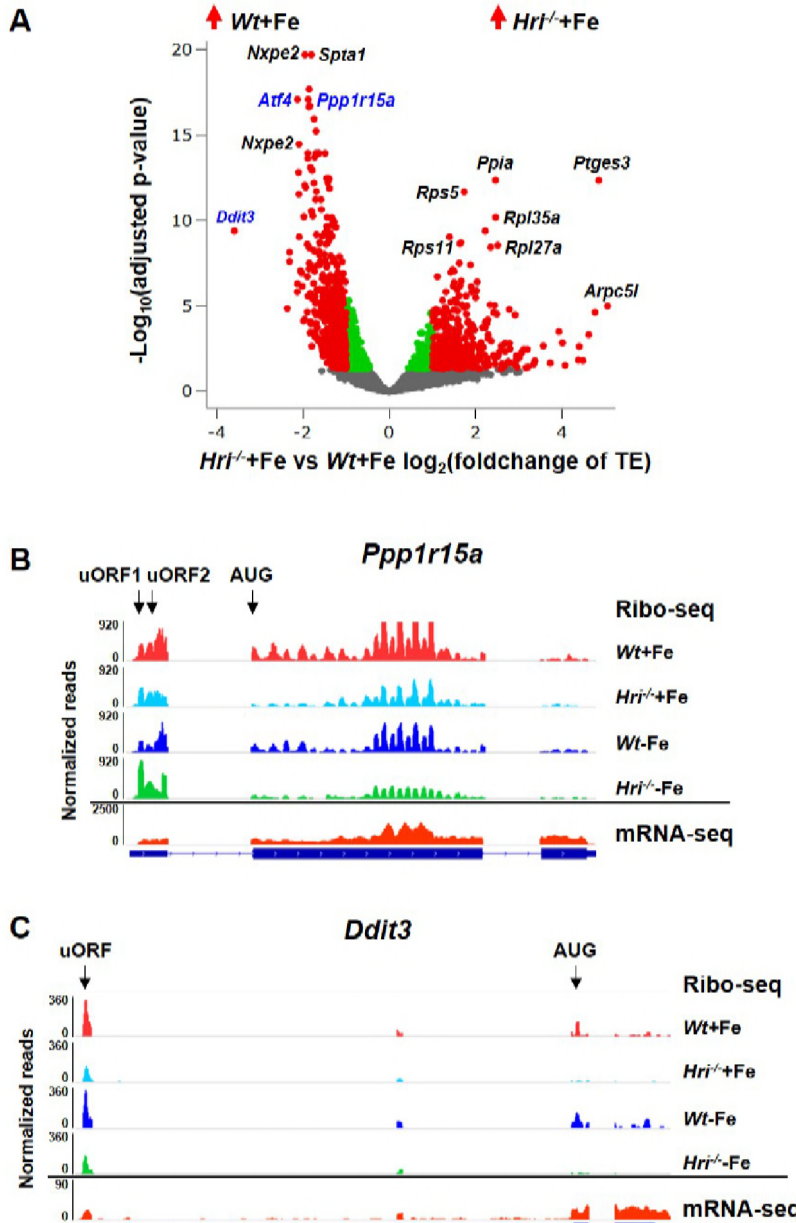
- 732 mRNA translation associated with eIF2 phosphorylation in erythroid progenitors."  
733 *PLOS ONE* 13 (4):e0193790. doi: 10.1371/journal.pone.0193790.
- 734 Patterson, A. D., M. C. Hollander, G. F. Miller, and A. J. Fornace, Jr. 2006. "Gadd34  
735 requirement for normal hemoglobin synthesis." *Mol Cell Biol* 26 (5):1644-53. doi:  
736 10.1128/mcb.26.5.1644-1653.2006.
- 737 Pavitt, G. D., and D. Ron. 2012. "New insights into translational regulation in the  
738 endoplasmic reticulum unfolded protein response." *Cold Spring Harb Perspect Biol* 4  
739 (6). doi: 10.1101/cshperspect.a012278.
- 740 Plasschaert, R. N., and M. S. Bartolomei. 2015. "Tissue-specific regulation and function  
741 of Grb10 during growth and neuronal commitment." *Proc Natl Acad Sci U S A* 112  
742 (22):6841-7. doi: 10.1073/pnas.1411254111.
- 743 Ramirez, F., D. P. Ryan, B. Gruning, V. Bhardwaj, F. Kilpert, A. S. Richter, S. Heyne, F.  
744 Dundar, and T. Manke. 2016. "deepTools2: a next generation web server for deep-  
745 sequencing data analysis." *Nucleic Acids Res* 44 (W1):W160-5. doi:  
746 10.1093/nar/gkw257.
- 747 Reimand, J., T. Arak, P. Adler, L. Kolberg, S. Reisberg, H. Peterson, and J. Vilo. 2016.  
748 "gProfiler-a web server for functional interpretation of gene lists (2016 update)." *Nucleic  
749 Acids Res* 44 (W1):W83-9. doi: 10.1093/nar/gkw199.
- 750 Ron, David, and Heather P. Harding. 2000. "Perk and Translational Control by Stress in  
751 Endoplasmic Reticulum." In *Translational Control of Gene Expression*, edited by J.W.B.  
752 Hershey, N. Sonenberg and M.B. Matthews, 547-60. Cold Springs Harbor: Cold Spring  
753 Harbor Laboratory Press.
- 754 Sankaran, V. G., L. S. Ludwig, E. Sicinska, J. Xu, D. E. Bauer, J. C. Eng, H. C. Patterson,  
755 R. A. Metcalf, Y. Natkunam, S. H. Orkin, P. Sicinski, E. S. Lander, and H. F. Lodish.  
756 2012. "Cyclin D3 coordinates the cell cycle during differentiation to regulate erythrocyte  
757 size and number." *Genes Dev* 26 (18):2075-87. doi: 10.1101/gad.197020.112.
- 758 Sankaran, Vijay G., and Stuart H. Orkin. 2013. "The Switch from Fetal to Adult  
759 Hemoglobin." *Cold Spring Harbor Perspectives in Medicine* 3 (1):a011643. doi:  
760 10.1101/cshperspect.a011643.
- 761 Scheuner, D., B. Song, E. McEwen, C. Liu, R. Laybutt, P. Gillespie, T. Saunders, S.  
762 Bonner-Weir, and R. J. Kaufman. 2001. "Translational control is required for the  
763 unfolded protein response and in vivo glucose homeostasis." *Mol Cell* 7 (6):1165-76.
- 764 Schranzhofer, M., M. Schiffrer, J. A. Cabrera, S. Kopp, P. Chiba, H. Beug, and E. W.  
765 Mullner. 2006. "Remodeling the regulation of iron metabolism during erythroid  
766 differentiation to ensure efficient heme biosynthesis." *Blood* 107 (10):4159-67. doi:  
767 10.1182/blood-2005-05-1809.
- 768 Singh, Seema, Arvind Dev, Rakesh Verma, Anamika Pradeep, Pradeep Sathyanarayana,  
769 Jennifer M. Green, Aishwarya Narayanan, and Don M. Wojchowski. 2012. "Defining  
770 an EPOR- Regulated Transcriptome for Primary Progenitors, including Tnfr-sf13c as a

- 771 Novel Mediator of EPO- Dependent Erythroblast Formation." *PLOS ONE* 7  
772 (7):e38530. doi: 10.1371/journal.pone.0038530.
- 773 Smith, F. M., L. J. Holt, A. S. Garfield, M. Charalambous, F. Koumanov, M. Perry, R.  
774 Bazzani, S. A. Sheardown, B. D. Hegarty, R. J. Lyons, G. J. Cooney, R. J. Daly, and A.  
775 Ward. 2007. "Mice with a disruption of the imprinted Grb10 gene exhibit altered body  
776 composition, glucose homeostasis, and insulin signaling during postnatal life." *Mol  
777 Cell Biol* 27 (16):5871-86. doi: 10.1128/mcb.02087-06.
- 778 Stonestrom, A. J., S. C. Hsu, K. S. Jahn, P. Huang, C. A. Keller, B. M. Giardine, S.  
779 Kadauke, A. E. Campbell, P. Evans, R. C. Hardison, and G. A. Blobel. 2015. "Functions  
780 of BET proteins in erythroid gene expression." *Blood* 125 (18):2825-34. doi:  
781 10.1182/blood-2014-10-607309.
- 782 Suragani, R. N., R. S. Zachariah, J. G. Velazquez, S. Liu, C. W. Sun, T. M. Townes, and  
783 J. J. Chen. 2012. "Heme-regulated eIF2alpha kinase activated Atf4 signaling pathway in  
784 oxidative stress and erythropoiesis." *Blood* 119 (22):5276-84. doi: 10.1182/blood-  
785 2011-10-388132.
- 786 Thom, C. S., E. A. Traxler, E. Khandros, J. M. Nickas, O. Y. Zhou, J. E. Lazarus, A. P.  
787 Silva, D. Prabhu, Y. Yao, C. Aribiana, S. Y. Fuchs, J. P. Mackay, E. L. Holzbaur, and  
788 M. J. Weiss. 2014. "Trim58 degrades Dynein and regulates terminal erythropoiesis."  
789 *Dev Cell* 30 (6):688-700. doi: 10.1016/j.devcel.2014.07.021.
- 790 Thoreen, C. C., L. Chantranupong, H. R. Keys, T. Wang, N. S. Gray, and D. M. Sabatini.  
791 2012. "A unifying model for mTORC1-mediated regulation of mRNA translation."  
792 *Nature* 485 (7396):109-13. doi: 10.1038/nature11083.
- 793 Ulirsch, J. C., J. N. Lacy, X. An, N. Mohandas, T. S. Mikkelsen, and V. G. Sankaran. 2014.  
794 "Altered chromatin occupancy of master regulators underlies evolutionary divergence in  
795 the transcriptional landscape of erythroid differentiation." *PLoS Genet* 10  
796 (12):e1004890. doi: 10.1371/journal.pgen.1004890.
- 797 Wang, L., B. Balas, C. Y. Christ-Roberts, R. Y. Kim, F. J. Ramos, C. K. Kikani, C. Li, C.  
798 Deng, S. Reyna, N. Musi, L. Q. Dong, R. A. DeFronzo, and F. Liu. 2007. "Peripheral  
799 disruption of the Grb10 gene enhances insulin signaling and sensitivity in vivo." *Mol  
800 Cell Biol* 27 (18):6497-505. doi: 10.1128/mcb.00679-07.
- 801 Wilkinson, Nicole, and Kostas Pantopoulos. 2013. "IRP1 regulates erythropoiesis and  
802 systemic iron homeostasis by controlling HIF2α mRNA translation." *Blood* 122  
803 (9):1658.
- 804 Xiao, Zhengtao, Qin Zou, Yu Liu, and Xuerui Yang. 2016. "Genome-wide assessment of  
805 differential translations with ribosome profiling data." *Nature Communications*  
806 7:11194. doi: 10.1038/ncomms11194  
807 <https://www.nature.com/articles/ncomms11194#supplementary-information>.
- 808 Yan, X., H. A. Himburg, K. Pohl, M. Quarmyne, E. Tran, Y. Zhang, T. Fang, J. Kan, N. J.  
809 Chao, L. Zhao, P. L. Doan, and J. P. Chute. 2016. "Deletion of the Imprinted Gene Grb10

- 810      Promotes Hematopoietic Stem Cell Self-Renewal and Regeneration." *Cell Rep* 17  
811      (6):1584-1594. doi: 10.1016/j.celrep.2016.10.025.
- 812      Zhang, Shuping, Alejandra Macias-Garcia, Jason Velazquez, Elena Paltrinieri, Randal J.  
813      Kaufman, and Jane-Jane Chen. 2018. "HRI coordinates translation by eIF2 $\alpha$ P and  
814      mTORC1 to mitigate ineffective erythropoiesis in mice during iron deficiency." *Blood*  
815      131 (4):450.
- 816

817 **Figure supplements**

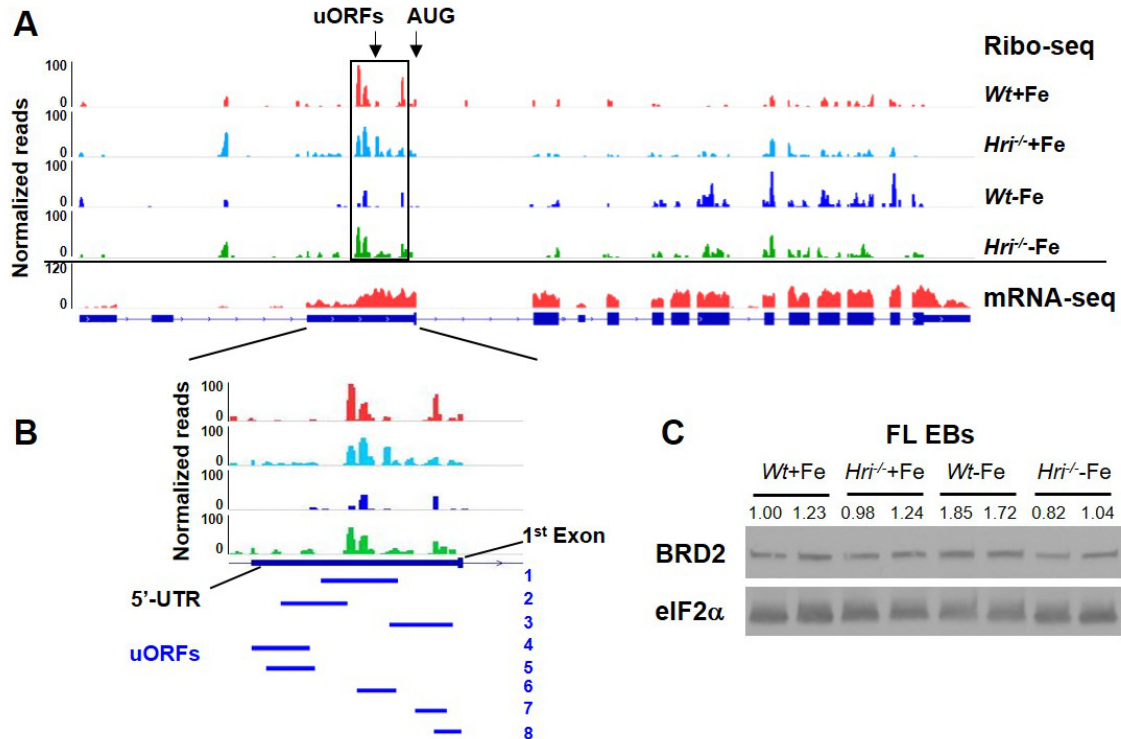
818 **Figure supplement 1. Translational regulation of ISR mRNAs by HRI**



819

820 **(A)** Increased translation of ISR mRNAs in *Wt+Fe* EBs compared to *Hri<sup>-/-</sup>+Fe* EBs. Red dots on the  
821 positive end of X-axis indicate significantly differentially translated mRNAs which are upregulated  
822 in *Hri<sup>-/-</sup>+Fe* EBs as compared to *Wt+Fe* EBs while red dots on the negative end of X-axis indicate  
823 those upregulated in *Wt+Fe* EBs as compared to *Hri<sup>-/-</sup>+Fe* EBs. Green and gray dots indicate not  
824 significantly differentially translated mRNAs. Genes labeled in blue indicate ISR mRNAs. TE,  
825 translational efficiency. **(B-C)** IGV-illustration of ribosome occupancies of the *Ppp1r15a* and *Ddit3*  
826 mRNAs. Mapped reads of mRNA-seq data from *Wt+Fe* EBs were shown only since no significant  
827 change at mRNA levels was observed among four samples.

828 **Figure supplement 2. Putative translational regulation of *Brd2* mRNA by HRI in ID**

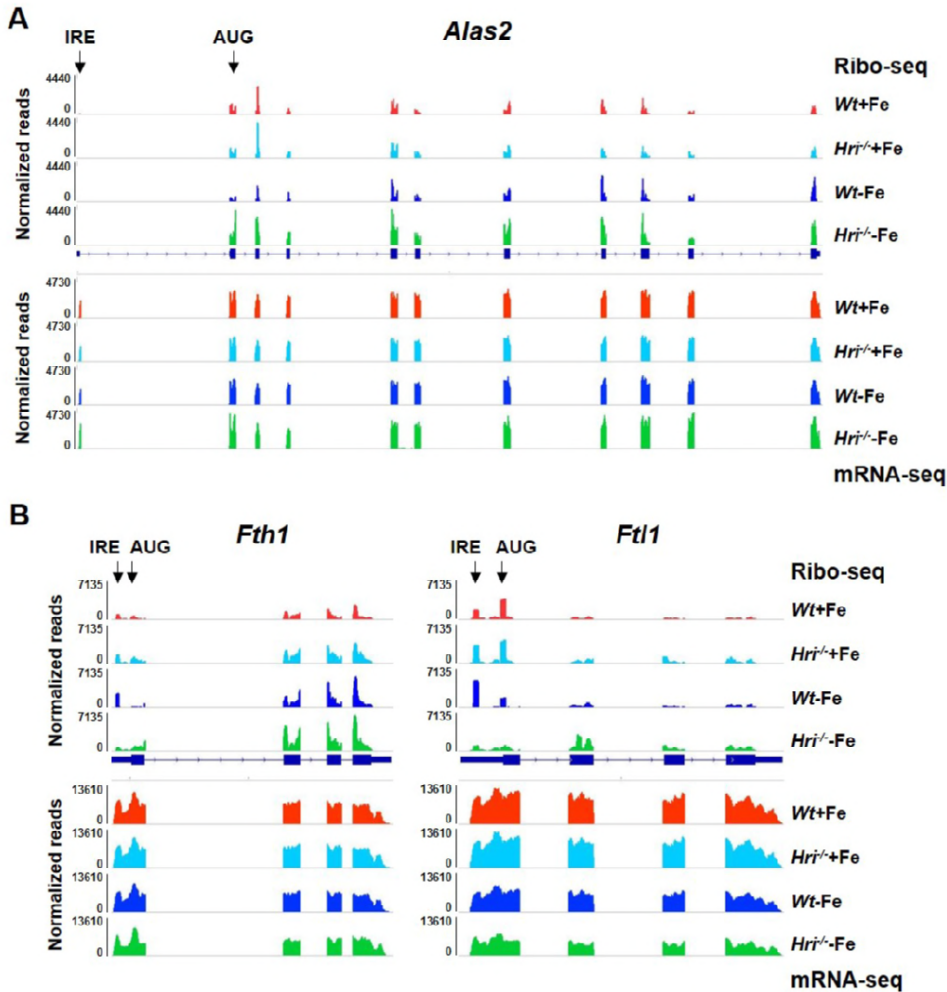


829

830 **(A)** IGV-illustration of ribosome occupancies of *Brd2* mRNA. **(B)** The enlarged view of the region  
831 containing the putative uORFs which were indicated by the blue lines. Only the second half of the  
832 5' UTR sequence (-1269 to +26) was analyzed for the prediction of the presence of putative uORFs  
833 due to the long length of whole UTR and the low ribosome density on the first half of 5' UTR. Eight  
834 uORFs were predicted, and ribosome occupancies were observed on all putative uORFs. **(C)** The  
835 protein levels of BRD2 in E14.5 FLs.

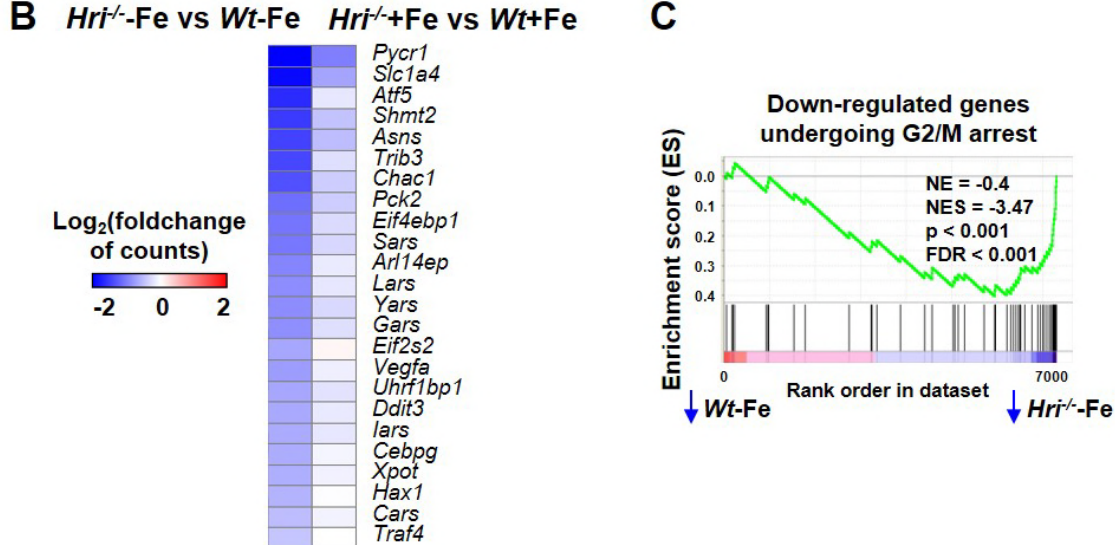
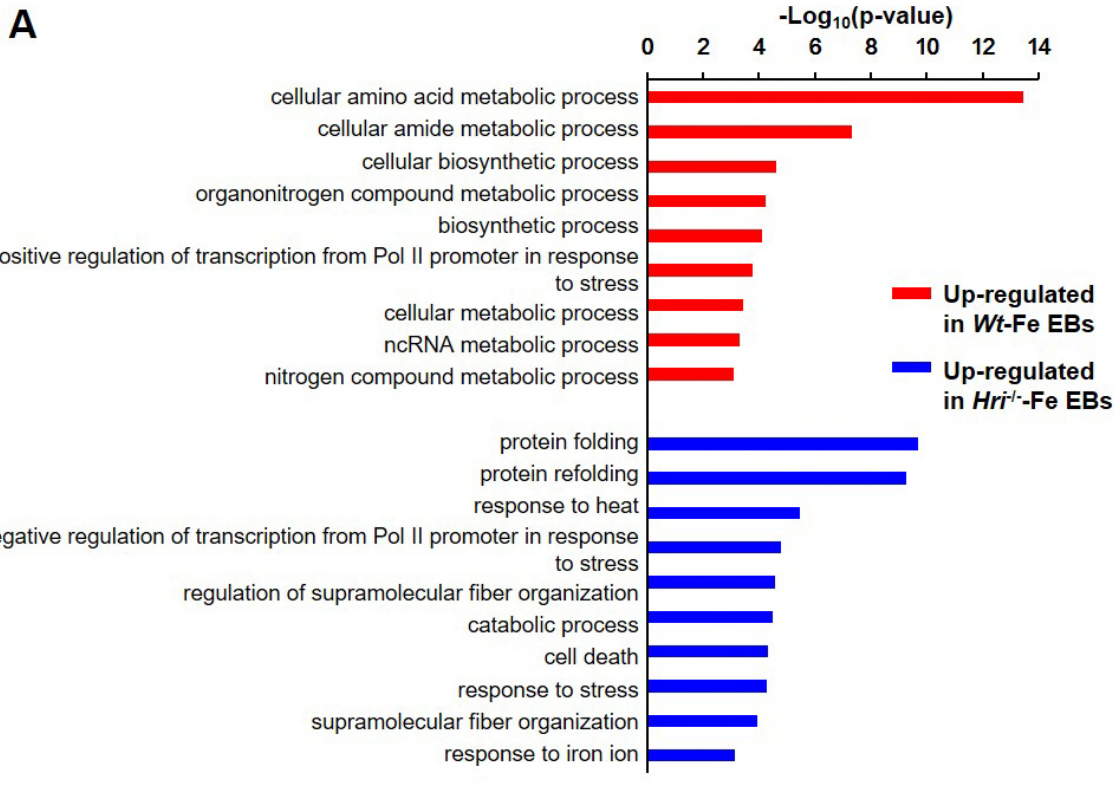
836

837 **Figure supplement 3. No significant alteration of translation of ALAS2 and ferritin  
838 mRNAs in ID**



839  
840      IGV-illustration of ribosome occupancies of **(A)** *Alas2*, and **(B)** *Fth1* and *Ftl1* mRNAs. These  
841      mRNAs contain IRE in 5'UTR and can be regulated translationally by IRPs.  
842

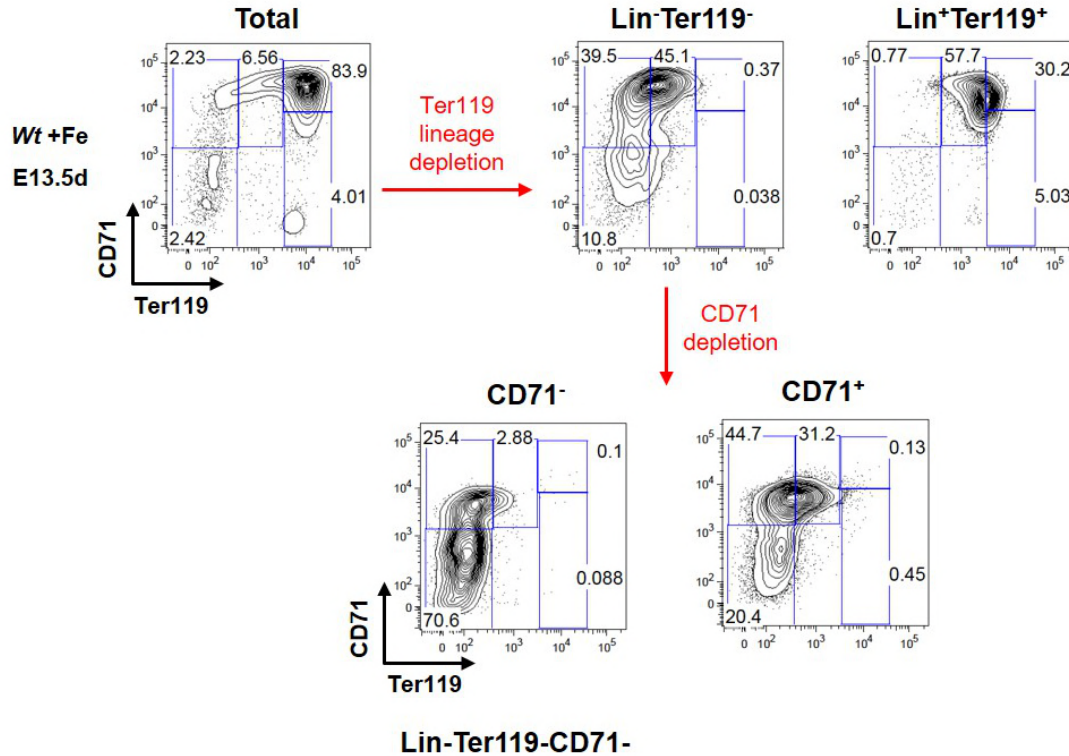
843 **Figure supplement 4. Analyses of differentially expressed mRNAs**



844

845 **(A)** GO analysis of significantly differentially expressed mRNAs between *Hri*<sup>-/-</sup>-Fe and *Wt*-Fe EBs.  
 846 **(B)** The heatmaps of differentially expressed ISR-target genes between *Hri*<sup>-/-</sup>-Fe and *Wt*-Fe EBs or  
 847 between *Hri*<sup>-/-</sup>+Fe and *Wt*+Fe EBs. **(C)** Gene Set Enrichment Analysis revealed G2/M arrest  
 848 pathway was downregulated in *Hri*<sup>-/-</sup>-Fe EBs as compared to *Wt*-Fe EBs.

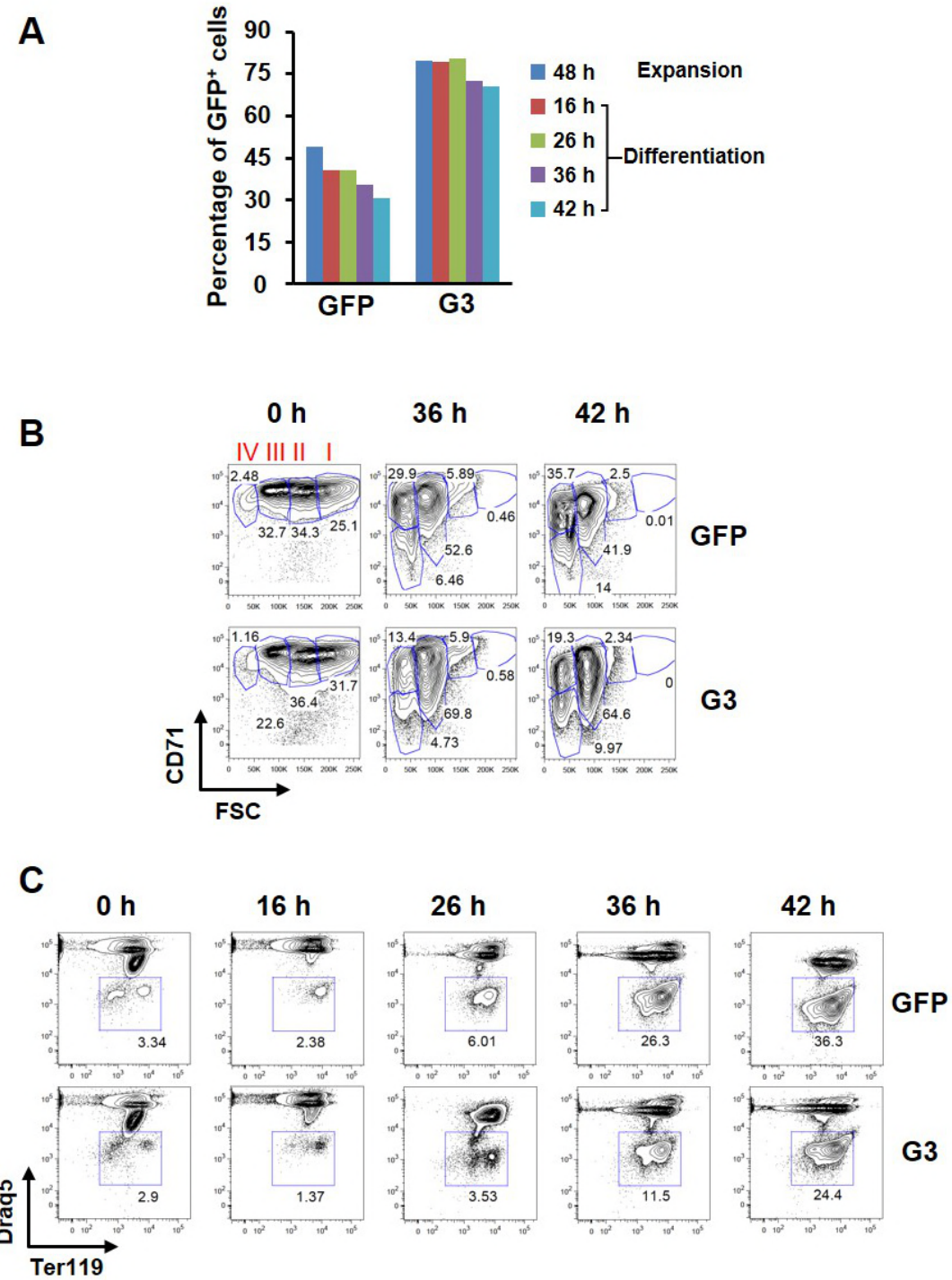
849 **Figure supplement 5. Enrichment of Lin<sup>-</sup>Ter119<sup>-</sup>CD71<sup>-</sup> erythroid progenitors from**  
850 **Wt+Fe E13.5 FLs for ex vivo experiments**



852

853

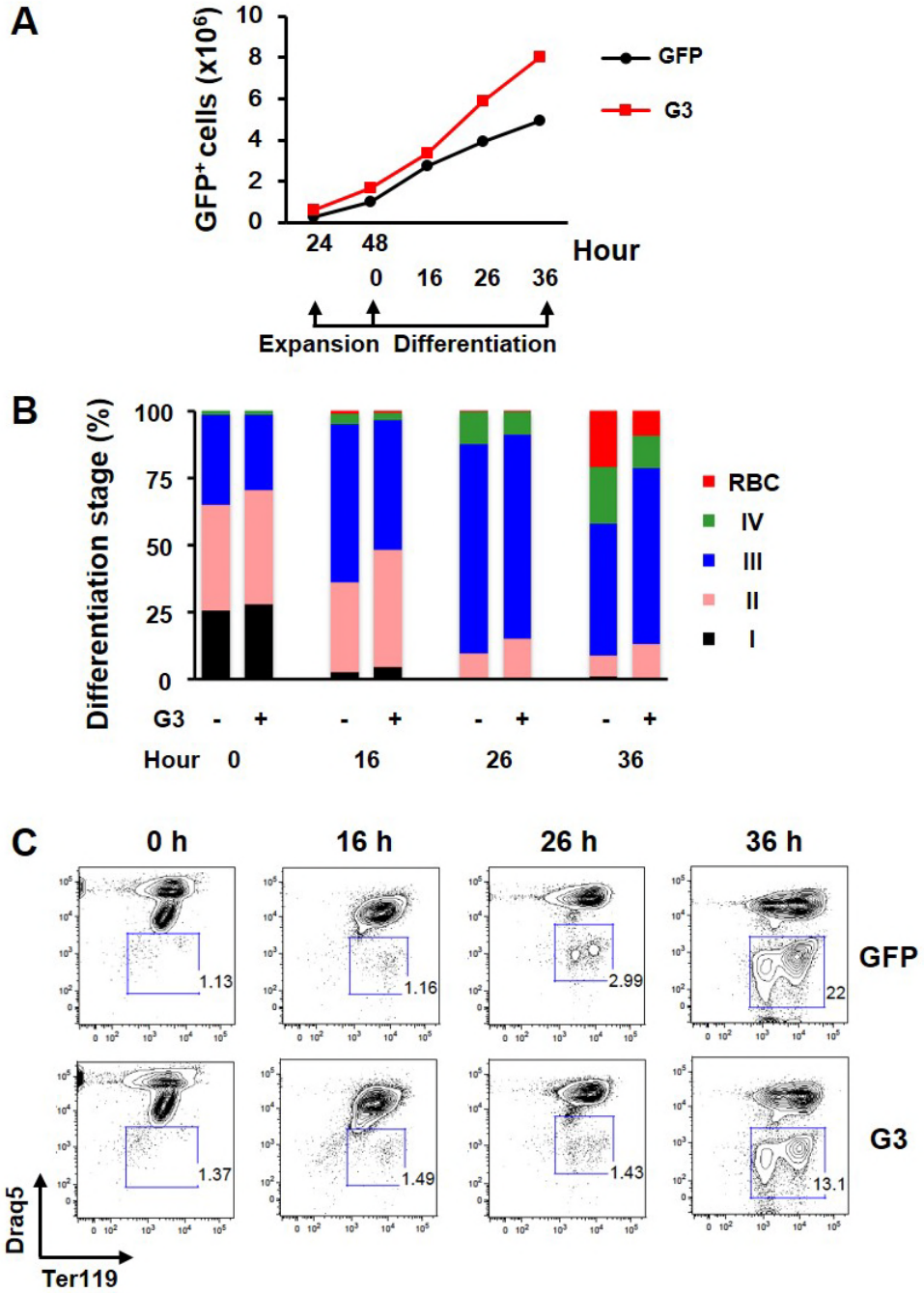
854 **Figure supplement 6. Effect of knockdown of *Grb10* on FL differentiation ex vivo**



855

856 **(A)** Percentages of  $\text{GFP}^+$  cells during expansion and differentiation phases after infection of GFP  
857 control and *Grb10* shRNA\_G3 recombinant retroviruses. **(B)** Representative plots of erythroid  
858 differentiation, corresponding to Figure 6D. **(C)** Enucleation of  $\text{GFP}^+$  cells during differentiation by  
859 flow cytometry using anti-Ter119 and Draq5 fluorescent dye.

860 **Figure supplement 7. Proliferation and differentiation of FL erythroid progenitors  
861 upon Grb10 knockdown**



862  
863 **(A)** The proliferation, **(B)** percentage of cells at erythroid differentiation stages, and **(C)** enucleation  
864 of GFP<sup>+</sup> cells after infection of GFP control and Grb10 shRNA\_G3 recombinant retroviruses. These  
865 results were obtained from an independent separate experiment from the results shown in Figure  
866 6.  
867

868 **Table supplements**

869 **Table supplement 1. Quality control and mapping of Ribo-seq and mRNA-seq**

Batch	Group	mRNA-seq			Ribo-seq				
		Reads (Million)	Uniquely mapped(%)	Mapped to multiple loci(%)	Length (bp)	%GC	Reads (Million)	Uniquely mapped(%)	Mapped to multiple loci(%)
1 <sup>st</sup> set	<i>Wt</i> +Fe	33.8	55.7	42.0	29	57	9.7	8.7	44.7
	<i>Wt</i> -Fe	62.5	68.8	29.4	28	55	18.1	9.4	33.5
	<i>Hri</i> <sup>-/-</sup> +Fe	55.6	62.6	35.2	29	56	41.1	7.6	44.3
	<i>Hri</i> <sup>-/-</sup> -Fe	66.6	63.5	34.6	29	56	33.7	9.1	40.4
2 <sup>nd</sup> set	<i>Wt</i> +Fe	42.5	58.8	39.2	30	55	21.5	20.8	52.6
	<i>Wt</i> -Fe	38.3	62.0	35.3	29	54	17.0	27.1	45.3
	<i>Hri</i> <sup>-/-</sup> +Fe	37.4	60.0	37.6	30	54	34.6	25.1	54.7
	<i>Hri</i> <sup>-/-</sup> -Fe	29.4	53.8	43.9	30	54	30.9	27.4	52.2
3 <sup>rd</sup> set	<i>Wt</i> +Fe	32.0	59.5	37.4					
	<i>Wt</i> -Fe	45.1	63.3	33.3					
	<i>Hri</i> <sup>-/-</sup> +Fe	42.8	59.8	37.7					
	<i>Hri</i> <sup>-/-</sup> -Fe	39.9	54.1	43.1					
	<i>Hri</i> <sup>-/-</sup> -Fe	46.5	61.9	35.9					

870 Higher reads obtained in the Ribo-seq data from *Hri*<sup>-/-</sup> EBs as compared to those from *Wt* EBs are  
871 consistent with the increased translation of *Hri*<sup>-/-</sup> cells (Han et al. 2001) since HRI inhibits translation.  
872

873 **Table supplement 2 Complete gene list of differentially translated mRNAs**

874 As determined using xtail package of R/Bioconductor, genes with reads greater than 50 at least in  
875 one of the conditions in each comparison were included in TE (translational efficiency) calculation.  
876 NA indicates that gene was not included in TE calculation due to reads below cut-off.  
877 Note: this table is a separate file in Excel format.

878

879 **Table supplement 3 Higher ribosome occupancy at the AUG of uORF1 in *Atf4***  
880 **mRNA**

Gene Symbol	Type	Condition	Ribo-seq/mRNA-seq	<i>Atf4/eIF2s1</i>	<i>Atf4/Rps6</i>
<i>Atf4</i>	uORF1	<i>Wt</i> +Fe	10.7	5.7	21.3
		<i>Hri</i> <sup>-</sup> +Fe	11.4	5.1	8.0
		<i>Wt</i> -Fe	7.2	5.0	15.4
		<i>Hri</i> <sup>-</sup> -Fe	20.3	12.8	13.5
<i>eIF2s1 (eIF2<math>\alpha</math>)</i>	Canonical ORF	<i>Wt</i> +Fe	1.9		
		<i>Hri</i> <sup>-</sup> +Fe	2.2		
		<i>Wt</i> -Fe	1.4		
		<i>Hri</i> <sup>-</sup> -Fe	1.6		
<i>Rps6</i>	Canonical ORF	<i>Wt</i> +Fe	0.5		
		<i>Hri</i> <sup>-</sup> +Fe	1.4		
		<i>Wt</i> -Fe	0.5		
		<i>Hri</i> <sup>-</sup> -Fe	1.5		

881 To calculate ribosome occupancy at AUG, Ribo-seq reads were normalized with the respective  
882 mRNA-seq reads. The AUG of uORF1 in *Atf4* mRNA was compared to the AUG of canonical ORFs  
883 of *eIF2s1 (eIF2 $\alpha$ )* and *Rps6*.

884

885 **Table supplement 4 No significant changes in TE of iron homeostasis-related genes**

Gene Symbol	IRE	Log2(FoldChange of TE)			
		<i>Hri</i> <sup>+/+Fe</sup> vs <i>Wt+Fe</i>	<i>Hri</i> <sup>-/-Fe</sup> vs <i>Wt-Fe</i>	<i>Wt-Fe</i> vs <i>Wt+Fe</i>	<i>Hri</i> <sup>-/-Fe</sup> vs <i>Hri</i> <sup>+/+Fe</sup>
<i>Ftl1</i>	5' UTR	0.05	1.18	-0.03	1.08
<i>Fth1</i>	5' UTR	-0.01	0.40	-0.12	0.26
<i>Alas2</i>	5' UTR	-0.66	0.27	-0.75	0.15
<i>Aco2</i>	5' UTR	-0.37	-0.14	0.22	0.44
<i>Slc40a1 (Fpn)</i>	5' UTR	-0.47	0.56	-0.39	0.61
<i>Tfrc (Tfr1)</i>	3' UTR	0.01	0.29	0.07	0.32
<i>Slc11a2 (Dmt1)</i>	3' UTR	0.15	0.14	0.21	0.18
<i>Slc25a37 (Mfrn1)</i>	NA	0.01	0.60	-0.61	-0.05
<i>Ncoa4</i>	NA	-0.53	1.19	-1.06	0.63
<i>Tfr2</i>	NA	-0.97	-0.16	-0.48	0.31
<i>Herc2</i>	NA	-1.89	-1.08	-0.92	-0.14

886 NA indicates no iron-responsive element (IRE). UTR, untranslated region. TE, translational  
887 efficiency.  
888

889 **Table supplement 5 Complete gene list of differentially expressed mRNAs**

890 As determined using DESeq2 package of R/Bioconductor, genes with the mean of reads of the  
891 conditions greater than 100 were used for further analysis.

892 Note: this table is a separate file in Excel format.

893

894 **Table supplement 6 DNA sequences of shRNA oligonucleotides**

No.	Oligo Sequence(5' to 3')
<i>Grb10</i> _shRNA1	aaaaCCAGAGTAATCCAAGGCGTTCTCGAGAACGCCCTTGGATTACTCTGG
<i>Grb10</i> _shRNA2	aaaaGCAGTTAAGAACTGCATCTCTCGAGAGAGATGCAGTTCTTAAC
<i>Grb10</i> _shRNA3	aaaaCCCTGGAATAACCTTGACAATCTCGAGATTGTCAAGGTTATTCCAGGG
<i>Grb10</i> _shRNA4	aaaaGCACACGGATGAATATCCTAACTCGAGTTAGGATATTCCGTGTGC
<i>Grb10</i> _shRNA5	aaaaCCATGCCAAGTGAGAGCAAATCTCGAGATTGCTCTCACTGGCATGG
Control_shRNA	aaaaCAACAAGATGAAGAGCACCAACTCGAGTTGGTGCTCTTCATCTGTTG

895

896 **Table supplement 7 DNA sequence of qPCR primers**

Gene symbol	Forward 5' to 3'	Reward 5' to 3'
<i>Grb10</i>	GTGGTGGAGATTCTAACCGACA	ACCTCTCTAATCCCAGTTGTGG
<i>Atf4</i>	GCCAGATGAGCTCTTGACCAC	CTGGAGTGGAGACAGAACCC
<i>Gapdh</i>	ATGGTGAAGGTCGGTGTGAA	GAGTGGAGTCATACTGGAAC

897

898 **Table supplement 8 List of antibodies used for Western blot analysis**

Symbol	Brand	Cat#
ATF4	Cell Signaling Technology	11815
GRB10	Millipore	07-2182
HRI	JJ Chen Lab	Han <i>et al.</i> , 2001
Cyclin D3	Cell Signaling Technology	2936
pAKT (Ser473)	Cell Signaling Technology	4060
AKT	Cell Signaling Technology	4691
β-Actin	Cell Signaling Technology	3700
eIF2α	Cell Signaling Technology	5324

899

900 **Method supplements**

901 **Library preparations of Ribo-seq**

902 To preserve polyribosomes, sorted EBs were washed twice with cold phosphate-  
903 buffered saline (PBS) and then treated with cycloheximide (100 µg/ml) at 37°C for 5 min,  
904 followed by isolation of RPFs as previously described (Guo et al. 2010, Ingolia, Lareau,  
905 and Weissman 2011) using ARTseq-Ribosome Profiling Kit (Illumina, San Diego, CA).  
906 Briefly, cells were lysed in cold polysome buffer on ice for 10 min. To generate RPFs,  
907 lysates were digested with Rnase 1. Monosomes were then purified by S-400 gel filtration  
908 spin columns (GE Healthcare, Chicago, IL). RNAs in monosomes were extracted, purified  
909 and followed by size selection of 28-34 nucleotides RPFs using denaturing polyacrylamide  
910 gel electrophoresis. Ribosomal RNA contaminants in the RPF preparations were removed  
911 using Ribo-Zero rRNA Removal Kit (Illumina, San Diego, CA). RPFs were then purified by  
912 15% urea-polyacrylamide gel electrophoresis. Libraries of RPFs were prepared as  
913 described (Ingolia et al. 2009, Ingolia, Lareau, and Weissman 2011) for Illumina next  
914 generation DNA sequencing. RPFs were dephosphorylated and linkers were ligated using  
915 T4 RNA ligase. RNA samples were then reverse transcribed, circularized and PCR  
916 amplified for 12 cycles. PCR products were subjected to gel purification before sequencing.  
917 Results of Ribo-seq presented in Figure 2 were from the second set of experiments. For  
918 the first set of Ribo-seq experiment, EBs were treated with harringtonine (2 µg/ml) at 37°C  
919 for 2 min followed by cycloheximide treatment as described above. However,

920 harringtonine treatment at this condition did not work well for EBs as ribosome  
921 occupancy was observed throughout many mRNAs. For the second set of Ribo-seq  
922 experiment, harringtonine was not used. Nonetheless, increased translation of *Atf4*,  
923 *Pppr115a* and *Ddit3* mRNAs was also observed in both sets of Ribo-seq.

924 **Genome-wide data analysis**

925 Raw data (fastq files) were trimmed by Cutadapt to remove adapters and reads with  
926 a base quality score less than 10. Reads with length less than 26 or 9 nucleotides were  
927 also discarded for Ribo-seq and mRNA-seq samples, respectively. For Ribo-seq samples,  
928 reads containing rRNA and tRNA sequences were further removed using Bowtie2. After  
929 quality control analysis using FastQC, reads were mapped to mouse genome mm10  
930 (UCSC) using STAR aligner with maxima of 2 mismatches and 8 multiple loci. Quality of  
931 Ribo-seq data was examined by the triplet periodicity using RibORF (Ji et al. 2015).

932 For the visualization of ribosome occupancies, all mapped reads (bam files) that  
933 overlap each bin (bin size = 1) were firstly calculated and normalized to effective mouse  
934 genome size to get a 1x depth of coverage (RPGC) using bamCoverage of deepTools  
935 (Ramirez et al. 2016). Then, ribosome occupancies were visualized using the Integrative  
936 Genomics Viewer (Broad Institute of Harvard and MIT). Since no significant change at  
937 mRNA levels among four conditions, only mapped reads of *Wt+Fe* EBs were shown for  
938 mRNA-seq data in Figure 2C-D, Figure 3C, Figure supplement 1B-C and Figure  
939 supplement 2A.

940       The uniquely mapped reads were counted using HTseq for gene coverage analysis,  
941       transcript per million (TPM) calculation, translational efficiency (TE) calculation and  
942       analysis of differentially expressed mRNAs (DEG). Genes with uniquely mapped reads  
943       greater than 25 in at least one of the conditions were used for gene coverage analysis and  
944       TPM calculation.

945       Generally, RPFs are piled up around the start codons and stop codons due to the  
946       slower kinetics of translation initiation and termination. The use of cycloheximide to freeze  
947       polysomes during the preparation of RPFs also enhances the pile up of reads near start  
948       codons. We, therefore, removed the first 15 and the last 5 codons from reads counting for  
949       the TE calculation of Ribo-seq data, in which TE is defined as the ratio of RPF counts to  
950       mRNA counts. TE was calculated using xtail package of R/Bioconductor, with parameter  
951       ‘bins = 10000’, to determine differentially translated genes between different conditions  
952       (Xiao et al. 2016). Genes with reads greater than 50 in at least one of the conditions were  
953       included in each comparison and were used for TE calculation (Table supplement 2).  
954       Genes with adjusted p-value < 0.05 together with  $\log_2(\text{foldchange of TE}) > 1.5$  or < -1.5  
955       were considered as significantly differentially translated in Figure 2A while adjusted p-  
956       value < 0.05 together with  $\log_2(\text{foldchange of TE}) > 1$  or < -1 were considered as  
957       significantly differentially translated in Figure 2B, Figure 3A, Figure 3D and Figure  
958       supplement 1A.

959 For Gene Set Enrichment Analysis (GSEA), pre-ranked gene lists were obtained  
960 using formula  $-\text{Log}_{10}(\text{adjusted p-value}) \times \text{Log}_2(\text{foldchange of TE})$ . Mouse gene symbols  
961 were converted into human symbols using biomaRt package of R/Bioconductor. GSEA  
962 was conducted using GSEA tool from Broad Institute with c2.all.v6.0.symbols.gmt  
963 database, which includes 4738 gene sets. Gene sets shown in Figure 3B were  
964 REACTOME\_FORMATION\_OF\_THE\_TERNARY\_COMPLEX\_AND\_SUBSEQUENTLY  
965 \_THE\_43S\_COMPL (rank 13), KEGG\_RIBOSOME (rank 1) and  
966 BILANES\_SERUM\_AND\_RAPAMYCIN\_SENSITIVE\_GENES (rank 9). Gene set  
967 shown in Figure supplement 4C was  
968 BHATI\_G2M\_ARREST\_BY\_2METHOXYESTRADIOL\_DN (rank 17).

969 Differentially expressed genes from mRNA-seq data were determined using DESeq2  
970 package of R/Bioconductor, and genes with the mean of reads of all conditions greater  
971 than 100 were used for further analysis (Table supplement 5). Genes with adjusted p-  
972 value < 0.05 were considered as significantly differentially expressed in Figure 4 and  
973 Figure supplement 4A-B. Lists of 5' TOP/TOP-like genes were obtained from Thoreen *et*  
974 *al* (Thoreen et al. 2012) while the integrated stress response (ISR) gene list was derived  
975 from Palam *et al* (Palam et al. 2015).

976 Gene ontology analysis was performed using g:Profiler (Reimand et al. 2016) for TE  
977 and DEG data sets. The START App was employed to generate the volcano plots, in  
978 which red dots indicate significantly differentially translated or expressed genes, while

979 green and gray dots indicate non significantly changed genes (Nelson et al. 2017).

980 Heatmaps were plotted using GENE-E tool from the Broad Institute.

981 **Purification of FL erythroid progenitors for ex vivo culture and differentiation**

982 In brief, total FL cells were mechanically dissociated by pipetting in PBS containing

983 2% FBS (Atlanta Biologicals, Norcross, GA), 2.5 mM EDTA and 10 mM glucose. Cells

984 were labeled with biotin-conjugated anti-B220, -CD3, -CD11b, -CD11c, -GR1, -Ter119

985 (BioLegend, San Diego, CA) and -CD41 (eBioscience, San Diego, CA) antibodies.

986 Lineage negative ( $\text{Lin}^- \text{Ter119}^-$ ) cells were subjected to a second purification step to obtain

987  $\text{Lin}^- \text{Ter119}^- \text{CD71}^-$  erythroid progenitors using biotin-conjugated anti-CD71 antibodies

988 (BioLegend, San Diego, CA and BD Biosciences, San Jose, CA).

989 Purified FL erythroid progenitors were expanded in StemPro-34 medium

990 complemented with 10% supplement, 2mM L-glutamine, 1% Penicillin-Streptomycin (P-

991  $10^{-4}$  M  $\beta$ -mercaptoethanol,  $10^{-6}$  M dexamethasone, 0.5 U/mL Epo, 100 ng/mL mouse

992 Stem Cell Factor (mSCF), and then differentiated in Iscove modified Dulbecco medium

993 (IMDM) containing 10% FCS (fetal calf serum, Gemini Bio-Products, West Sacramento,

994 CA), 10% plasma derived serum (Animal Technologies, Tyler, TX), 2 mM L-glutamine, 1%

995 P-S,  $10^{-4}$  M  $\beta$ -mercaptoethanol, 5 U/mL Epo.